

Explicit construction of entropy solutions for the Lighthill-Whitham-Richards traffic flow model with a non-smooth flow-density relationship

Yadong Lu¹, S.C. Wong², Mengping Zhang³, Chi-Wang Shu⁴ and Wenqin Chen⁵

Abstract

In this paper we explicitly construct the entropy solutions for the Lighthill-Whitham-Richards (LWR) traffic flow model with a flow-density relationship $q(\rho)$ which is piecewise quadratic, continuous, concave, but not differentiable at the junction points where two quadratic polynomials meet, and with piecewise linear initial condition and piecewise constant boundary conditions. As observed traffic flow data can be well fitted with such continuous piecewise quadratic functions, the explicitly constructed solutions provide a fast and accurate solution tool which may be used for predicting traffic or as a diagnosing tool to test the performance of numerical schemes. We implement these explicit entropy solutions for three representative traffic flow cases and also compare them with numerical solutions obtained by a high order weighted essentially non-oscillatory (WENO) scheme.

Key Words: LWR model; traffic flow; non-smooth flow-density relationship; entropy solution, WENO scheme

¹Department of Mathematics, University of Science and Technology of China, Hefei, Anhui 230026, China. E-mail: luyd@mail.ustc.edu.cn.

²Department of Civil Engineering, The University of Hong Kong, Hong Kong, China. E-mail: hhewsc@hkucc.hku.hk.

³Department of Mathematics, University of Science and Technology of China, Hefei, Anhui 230026, China. E-mail: mpzhang@ustc.edu.cn.

⁴Division of Applied Mathematics, Brown University, Providence, RI 02912, USA. E-mail: shu@dam.brown.edu.

⁵Department of Civil Engineering, The University of Hong Kong, Hong Kong, China. E-mail: manyen@hku.hk.

1 Introduction

One of the earliest studies of traffic flow theory began when Greenshields (1934) measured the traffic flow and speed on a highway and identified a linear relationship between speed and density. To describe the dynamic characteristics of traffic on a homogeneous and unidirectional highway, Lighthill and Whitham (1955) and Richards (1956) independently proposed a macroscopic model of traffic flow, which is now known as the LWR model in the literature of traffic flow theory. Since then, a substantial amount of work has been conducted to improve the modeling approach of traffic flows, which can be broadly classified as hydrodynamic models (Daganzo, 1994; Kerner and Konhauser, 1994; Newell, 1993; Payne, 1979; Zhang, 1998; Wong and Wong, 2002a), gas kinetic models (Helbing, 1996; Hoogendoorn and Bovy, 2000; Nelson and Sopasakis, 1998; Prigogine and Herman, 1971; Pavieri-Fontana, 1975), and cellular automation models (Biham et al., 1992; Cuesta et al., 1993; Krauss et al., 1997; Nagatani, 1993; Nagel and Schreckenberg, 1992). Although advances have been made in many directions, the LWR model is still widely used for the modeling of traffic flow, because of its simplicity and good explanatory power to understand the qualitative behavior of road traffic. The results that are obtained from the LWR model are generally adequate for many applications such as traffic management and control problems.

The LWR model is formulated as a scalar hyperbolic conservation law and is often solved by finite difference methods (Daganzo, 1995; LeVeque, 1992; Lebacque, 1996; Michalopoulos et al., 1984). The main difficulty in designing efficient and high order finite difference methods for the LWR model or in general for hyperbolic conservation laws is the inherent presence of discontinuities (shocks) in the solution (Lebacque, 1996). Moreover, discontinuous weak solutions are not unique for hyperbolic conservation laws and entropy conditions must be satisfied to obtain physically valid solution that is consistent with human behavior (such as the driver's ride impulse) (Ansorge, 1990; Velan and Florian, 2002). For some specific forms of the equilibrium flow-density relationship, the LWR model can be solved analytically (Haberman, 1977; Whitham, 1974). Recently, the analytical solution for a specific class of

LWR model was derived, which assumed that the flow-density relationship is governed by a quadratic function throughout the density regime (Wong and Wong, 2002b). However, from many observations, this assumption is too strong for general applications. Therefore, it is natural to extend the method to the case with a more general flow-density relationship. In the traffic flow literature, it is not uncommon to divide the range of the density into a number of regimes, within each of which a flow-density curve is fitted with the observed data (Dick, 1966; Edie, 1961; May and Keller, 1968; Underwood, 1961). In this paper, we assume that the flow-density relationship is concave and is represented by a piecewise quadratic function, with any two adjacent pieces joining continuously at a critical density ρ_c but with a discontinuous first derivative at ρ_c . Thus the considered flow-density relationship is only Lipschitz continuous but not everywhere differentiable. For such type of flow-density relationships, the entropy solution still exists and is unique for general bounded variation initial conditions (Dafermos, 1972). We obtain in Section 2 explicit formulas for the entropy solutions with such flow-density relationship and with piecewise linear initial condition and piecewise constant boundary conditions. In Section 3 we summarize the solution procedure, concentrating on the discussion of finding the earliest time when the waves (characteristic lines or shocks) from the previous initial condition intersect with one another and hence the construction of the entropy solution must be restarted based on a new piecewise linear initial data. In Section 4 we provide numerical examples in traffic flows to demonstrate the explicit solutions obtained in Section 2. We also compare these explicit solutions with numerical solutions obtained by using the high order weighted essentially non-oscillatory (WENO) schemes (Jiang and Shu, 1996; Zhang et al., 2003). Concluding remarks are given in Section 5.

2 Explicit construction of the entropy solutions

The governing equation for the LWR model is the following scalar hyperbolic conservation law

$$\rho_t + q(\rho)_x = 0 \quad (1)$$

with suitable initial and boundary conditions. Here $\rho \in (0, \rho_{\max})$ is the density, ρ_{\max} is the maximum (jam) density, and $q(\rho)$ is the traffic flow on a homogeneous highway, which is assumed to be a function of the density ρ only in the LWR model. More specifically, the flow q , the density ρ and the equilibrium speed u are related by

$$q(\rho) = u(\rho) \rho. \quad (2)$$

In this paper, the flow $q(\rho)$ is considered to be continuous, piecewise quadratic, and concave. Without loss of generality, we will concentrate our discussion on the situation where the flow q is defined by two different quadratic functions in different regimes

$$q(\rho) = \begin{cases} q_1(\rho), & 0 \leq \rho \leq \rho_c \\ q_2(\rho), & \rho_c \leq \rho \leq \rho_{\max} \end{cases} \quad (3)$$

where

$$\text{Flux I: } q_1(\rho) = d_0 + d_1 \rho + d_2 \rho^2; \quad \text{Flux II: } q_2(\rho) = e_0 + e_1 \rho + e_2 \rho^2 \quad (4)$$

are two different quadratic functions, which are continuous at the junction $q_1(\rho_c) = q_2(\rho_c)$, concave in each piece $q_1''(\rho) < 0$ and $q_2''(\rho) < 0$, and concave also at the junction $q_1'(\rho_c) \geq q_2'(\rho_c)$. A typical flow in this setup is given in Figure 1. The general situation of the flow q with more than two pieces of quadratic functions can be considered with the same recipe to each neighboring pairs of quadratic flow functions.

We now start the construction of explicit solutions to the conservation law (1) with such flows $q(\rho)$, when the initial condition is piecewise linear. We will first ignore the boundary conditions, and will leave the discussion of the treatment of piecewise constant boundary conditions to Sections 2.3 and 2.4. We begin with the generalized Riemann problem

$$\rho(x, 0) = \begin{cases} \alpha_1 + \beta_1 x, & x < 0 \\ \alpha_2 + \beta_2 x, & x \geq 0 \end{cases}. \quad (5)$$

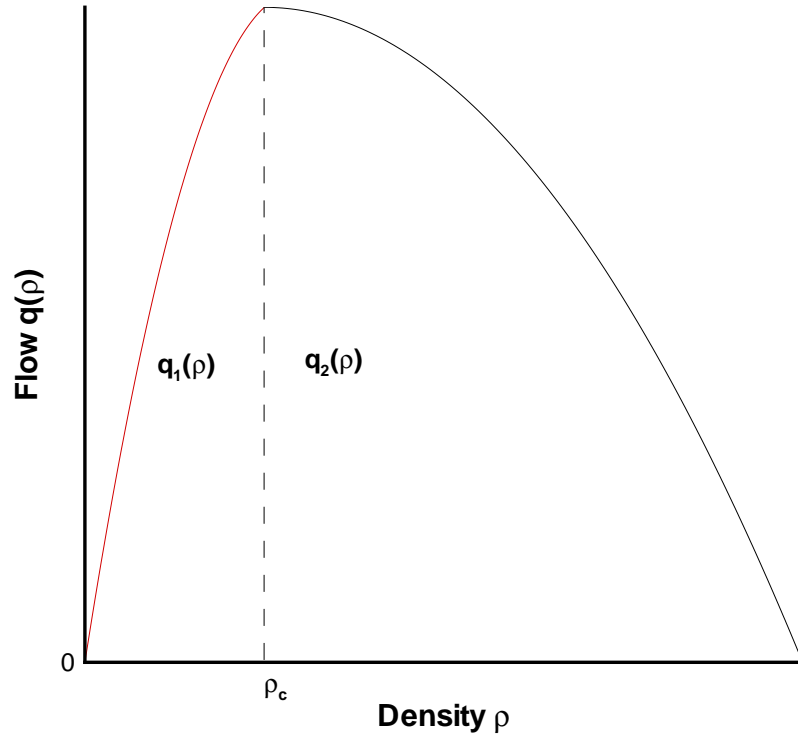


Figure 1: A typical flow with two different concave quadratic functions joining continuously at a critical density ρ_c with discontinuous and decreasing derivative at ρ_c .

We also assume that, for the x range we are considering, the initial density $\alpha_i + \beta_i x$ is completely contained in one of the regimes $\rho \leq \rho_c$ or $\rho \geq \rho_c$ for $i = 1$ and 2. This does not lose generality, as we can break a single linear function into two pieces as in (5) when it crosses the critical density ρ_c . We also remark that we do not need to consider the case when both linear functions $\alpha_i + \beta_i x$, for $i = 1, 2$, are contained in a single regime $\rho \leq \rho_c$ or $\rho \geq \rho_c$, because this is covered by the results in (Wong and Wong, 2002b).

Before solving the generalized Riemann problem, we write down a simple but important fact that we will heavily use in the sequel. For the scalar conservation law (1) with a quadratic flux $q(\rho) = a + b\rho + c\rho^2$ and a linear initial condition $\rho(x, 0) = \alpha + \beta x$, the solution stays linear

$$\rho(x, t) = \alpha(t) + \beta(t)x \tag{6}$$

with

$$\alpha(t) = \frac{\alpha - b\beta t}{1 + 2c\beta t}, \quad \beta(t) = \frac{\beta}{1 + 2c\beta t}. \quad (7)$$

This can be easily obtained by the method of characteristics and we can easily check that (6) with (7) is a smooth solution to the conservation law (1) with the initial condition $\rho(x, 0) = \alpha + \beta x$, until it becomes singular (i.e. until the denominator $1 + 2c\beta t = 0$). This simple fact is the main reason that enables us to obtain explicit formulas for the entropy solution. The solution for each linear piece of the initial condition is given by (6)-(7) until neighboring waves interact with each other.

We now assume that the x -axis is divided into a number of intervals, within each of them the initial density is given by a linear function $\rho(x, 0) = \alpha + \beta x$ which is completely contained in one of the regimes $\rho \leq \rho_c$ or $\rho \geq \rho_c$. We consider the solution to the generalized Riemann problem (1) with the initial condition (5) for each of the inner boundary points separating two piecewise linear initial conditions. The left and right intervals to the inner boundary point under consideration are denoted by

$$\mathbf{e} = (x_l, x_r), \quad \bar{\mathbf{e}} = (\bar{x}_l, \bar{x}_r)$$

respectively, with clearly $x_r = \bar{x}_l$. The initial condition density values at the relevant interval boundaries are denoted by

$$\rho_l = \rho(x_l^+, 0), \quad \rho_r = \rho(x_r^-, 0); \quad \bar{\rho}_l = \rho(\bar{x}_l^+, 0), \quad \bar{\rho}_r = \rho(\bar{x}_r^-, 0)$$

see Figure 2. Notice that the exact solution is obtained only to the smallest time when the waves (characteristic lines or shocks) from the initial condition intersect with one another. At this time the new piecewise linear initial condition is formed and the procedure is repeated. We consider the following situations separately.

2.1 Propagation of a shock

If $\rho_r \leq \rho_c \leq \bar{\rho}_l$ and the intervals \mathbf{e} and $\bar{\mathbf{e}}$ belong to Flux I and Flux II in (4) respectively, as shown in Figure 2, then a shock satisfying the Lax entropy condition (Lax, 1973) is

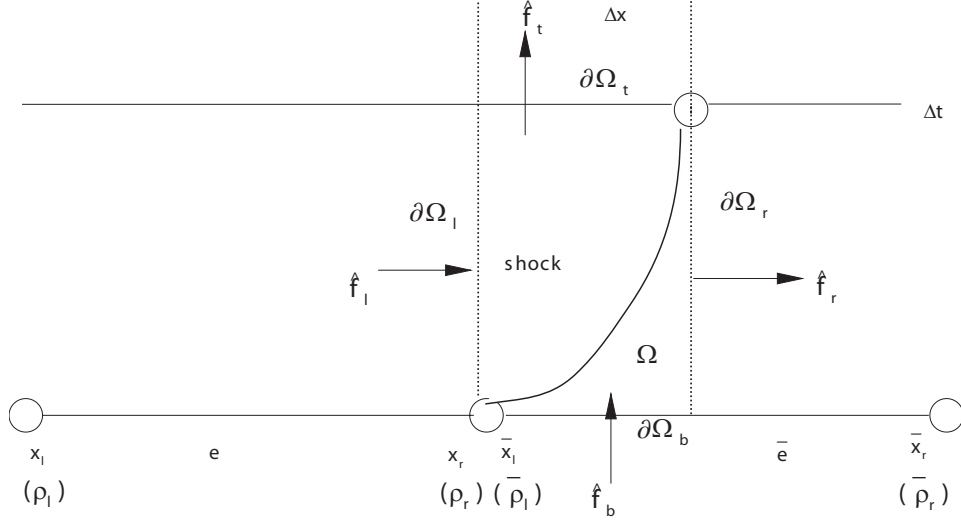


Figure 2: Propagation of a right-moving shock from a nodal point.

generated from the point $x_r = \bar{x}_l$ and will move to the right or left along a curve determined by the Rankine-Hugoniot jump condition. If the shock moves to the right, an easy way to determine the location of the shock $\bar{x}_l + \Delta x$ after time Δt is through conservation in the rectangular region Ω with $(\bar{x}_l, 0)$ and $(\bar{x}_l + \Delta x, \Delta t)$ as the end points of a diagonal (see Figure 2). Notice that, as we consider only the time Δt smaller than the smallest time when the waves (characteristic lines or shocks) from the initial condition intersect with one another, we may safely assume that the left and top boundaries of this rectangle, $\partial\Omega_l$ and $\partial\Omega_t$, belong to Flux I, and the right and bottom boundaries of this rectangle, $\partial\Omega_r$ and $\partial\Omega_b$, belong to Flux II.

The flux at the left boundary $\partial\Omega_l$, namely the number of vehicles coming from the left

boundary into the region Ω during time period Δt is

$$\hat{f}_l = \int_0^{\Delta t} q_1|_{x=x_r} dt = \int_0^{\Delta t} [d_0 + d_1(\alpha_1(t) + \beta_1(t)x_r) + d_2(\alpha_1(t) + \beta_1(t)x_r)^2] dt \quad (8)$$

where $\alpha_1(t)$ and $\beta_1(t)$ are given by (7) with α and β replaced by α_1 and β_1 in the initial condition (5). Likewise, the flux at the right boundary $\partial\Omega_r$, namely the number of vehicles leaving the right boundary from the region Ω is

$$\begin{aligned} \hat{f}_r &= \int_0^{\Delta t} q_2|_{x=\bar{x}_l+\Delta x} dt \\ &= \int_0^{\Delta t} [e_0 + e_1(\alpha_2(t) + \beta_2(t)(\bar{x}_l + \Delta x)) + e_2(\alpha_2(t) + \beta_2(t)(\bar{x}_l + \Delta x))^2] dt. \end{aligned} \quad (9)$$

The initial number of vehicles within the region Ω at time $t = 0$ is

$$\hat{f}_b = \int_{\bar{x}_l}^{\bar{x}_l+\Delta x} (\alpha_2(0) + \beta_2(0)x) dx \quad (10)$$

and the final number of vehicles within the region Ω at time $t = \Delta t$ is

$$\hat{f}_t = \int_{x_r}^{x_r+\Delta x} (\alpha_1(\Delta t) + \beta_1(\Delta t)x) dx. \quad (11)$$

From the flow conservation principle, we deduce that

$$\hat{f}_l - \hat{f}_r + \hat{f}_b - \hat{f}_t = 0. \quad (12)$$

Using the explicit formulas (6)-(7), we obtain from (12) the explicit equation determining Δx as

$$F_1(\Delta t) \Delta x^2 + F_2(\Delta t) \Delta x + F_3(\Delta t) = 0 \quad (13)$$

where

$$\begin{aligned} F_1(\Delta t) &= \{2\Delta t(d_2 - e_2)(\rho_r - \rho_l)(\bar{\rho}_r - \bar{\rho}_l) + (x_r - x_l)(\bar{\rho}_r - \bar{\rho}_l) - (\bar{x}_r - \bar{x}_l)(\rho_r - \rho_l)\} / \\ &\quad \{2 [2d_2\Delta t(\rho_l - \rho_r) + x_l - x_r] [2e_2\Delta t(\bar{\rho}_l - \bar{\rho}_r) + \bar{x}_l - \bar{x}_r]\} \end{aligned}$$

$$\begin{aligned} F_2(\Delta t) &= \{-(x_l - x_r)[\Delta t(e_1 + 2e_2\rho_r)(\bar{\rho}_l - \bar{\rho}_r) - (\bar{\rho}_l - \rho_r)(\bar{x}_l - \bar{x}_r)] + d_1\Delta t(\rho_l - \rho_r)[2e_2\Delta t(\bar{\rho}_l - \bar{\rho}_r) \\ &\quad + \bar{x}_l - \bar{x}_r] - 2d_2\Delta t(\rho_l - \rho_r)[\Delta t e_1(\bar{\rho}_l - \bar{\rho}_r) - \bar{\rho}_l(\bar{x}_l - \bar{x}_r)]\} / \\ &\quad \{[2d_2\Delta t(\rho_l - \rho_r) + x_l - x_r][2e_2\Delta t(\bar{\rho}_l - \bar{\rho}_r) + \bar{x}_l - \bar{x}_r]\} \end{aligned}$$

$$\begin{aligned}
F_3(\Delta t) = & \left\{ \Delta t \{ (x_l - x_r) \{ \Delta t [e_1^2 + 4(d_0 - e_0)e_2] (\bar{\rho}_l - \bar{\rho}_r) + 2(d_0 - e_0 - e_1\bar{\rho}_l - e_2\bar{\rho}_l^2) (\bar{x}_l - \bar{x}_r) \} \right. \\
& + 2d_2 \{ \Delta t^2 [e_1^2 + 4(d_0 - e_0)e_2] (\rho_l - \rho_r) (\bar{\rho}_l - \bar{\rho}_r) + 2\Delta t \{ e_2 [\bar{\rho}_l \rho_r^2 (x_l - x_r) + \rho_r^2 \bar{\rho}_r (x_r - x_l) \\
& - \bar{\rho}_l^2 (\rho_l - \rho_r) (\bar{x}_l - \bar{x}_r)] + (d_0 - e_0 - e_1\bar{\rho}_l) (\rho_l - \rho_r) (\bar{x}_l - \bar{x}_r) \} + \rho_r^2 (x_l - x_r) (\bar{x}_l - \bar{x}_r) \} \\
& - d_1^2 \Delta t (\rho_l - \rho_r) [2\Delta t e_2 (\bar{\rho}_l - \bar{\rho}_r) + \bar{x}_l - \bar{x}_r] + 2d_1 \rho_r (x_l - x_r) (2\Delta t e_2 (\bar{\rho}_l - \bar{\rho}_r) + \bar{x}_l - \bar{x}_r) \} \} \\
& / \{ 2[2d_2 \Delta t (\rho_l - \rho_r) + x_l - x_r] [2e_2 \Delta t (\bar{\rho}_l - \bar{\rho}_r) + \bar{x}_l - \bar{x}_r] \}
\end{aligned}$$

The shock trajectory can therefore be determined by solving the quadratic equation (13)

$$\Delta x = \frac{-F_2(\Delta t) + \sqrt{\Delta}}{2F_1(\Delta t)} \quad (14)$$

where $\Delta = F_2(\Delta t)^2 - 4F_1(\Delta t)F_3(\Delta t)$. If the root Δx determined by (14) is negative, then the assumption of a right-moving shock is incorrect. In this case, we can determine the location of the shock $\bar{x}_l + \Delta x$ after time Δt again through conservation in the rectangular region $\tilde{\Omega}$ with $(\bar{x}_l, 0)$ and $(\bar{x}_l + \Delta x, \Delta t)$ as the end points of a diagonal (see Figure 3). We may again safely assume that the left and bottom boundaries of this rectangle, $\partial\Omega_l$ and $\partial\Omega_b$, belong to Flux I, and the right and top boundaries of this rectangle, $\partial\Omega_r$ and $\partial\Omega_t$, belong to Flux II. The left and right fluxes \hat{f}_l and \hat{f}_r are changed to

$$\begin{aligned}
\hat{f}_l &= \int_0^{\Delta t} q_1|_{x=x_r+\Delta x} dt \\
&= \int_0^{\Delta t} [d_0 + d_1(\alpha_1(t) + \beta_1(t)(x_r + \Delta x)) + d_2(\alpha_1(t) + \beta_1(t)(x_r + \Delta x))^2] dt \quad (15)
\end{aligned}$$

and

$$\hat{f}_r = \int_0^{\Delta t} q_2|_{x=\bar{x}_l} dt = \int_0^{\Delta t} [e_0 + e_1(\alpha_2(t) + \beta_2(t)\bar{x}_l) + e_2(\alpha_2(t) + \beta_2(t)\bar{x}_l)^2] dt \quad (16)$$

respectively. The bottom and top fluxes are changed to

$$\hat{f}_b = \int_{x_r}^{x_r+\Delta x} (\alpha_1(0) + \beta_1(0)x) dx; \quad (17)$$

and

$$\hat{f}_t = \int_{\bar{x}_l}^{\bar{x}_l+\Delta x} (\alpha_2(\Delta t) + \beta_2(\Delta t)x) dx. \quad (18)$$

In this case, the flow conservation principle (12) yields the explicit equation determining Δx as

$$\tilde{F}_1(\Delta t) \Delta x^2 + \tilde{F}_2(\Delta t) \Delta x + \tilde{F}_3(\Delta t) = 0 \quad (19)$$

where we can easily check that $\tilde{F}_i(\Delta t) = -F_i(\Delta t)$, $i = 1, 2, 3$. Therefore the shock trajectory can be determined by solving the quadratic equation (19)

$$\Delta x = \frac{-\tilde{F}_2(\Delta t) - \sqrt{\Delta}}{2\tilde{F}_1(\Delta t)} = \frac{-F_2(\Delta t) + \sqrt{\Delta}}{2F_1(\Delta t)} \quad (20)$$

where $\Delta = \tilde{F}_2(\Delta t)^2 - 4\tilde{F}_1(\Delta t)\tilde{F}_3(\Delta t) = F_2(\Delta t)^2 - 4F_1(\Delta t)F_3(\Delta t)$. Notice that the formulas (14) and (20) are identical so we do not need to decide *a priori* whether the shock moves to the left or right.

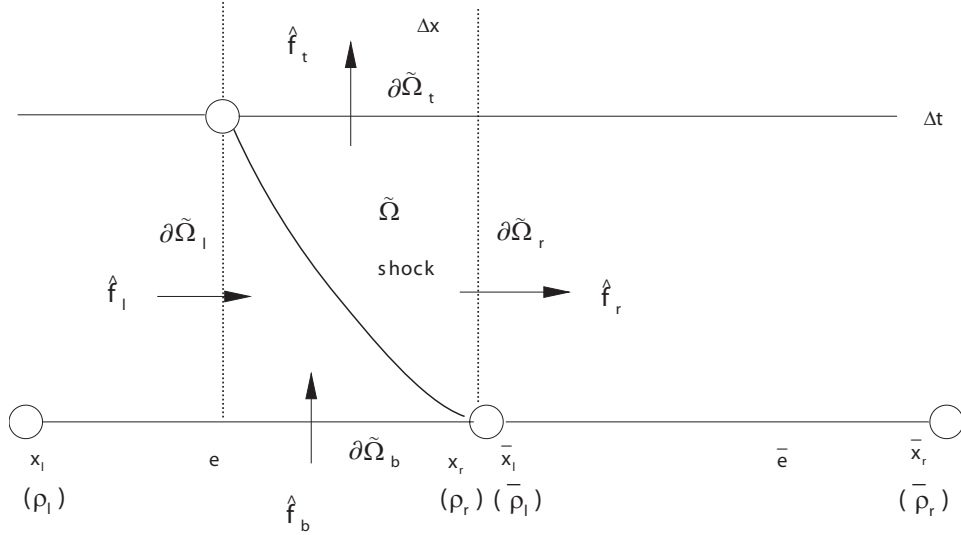


Figure 3: Propagation of a left-moving shock from a nodal point.

2.2 Propagation of a rarefaction wave

If $\rho_r \geq \rho_c \geq \bar{\rho}_l$ and the intervals \mathbf{e} and $\bar{\mathbf{e}}$ belong to Flux II and Flux I in (4) respectively, then a rarefaction wave is generated and three new intervals \mathbf{e}_1 , \mathbf{e}_2 and \mathbf{e}_3 are created at the time $t = \Delta t$, as shown in Figure 4. We again consider only the time Δt smaller than the smallest time when the waves (characteristic lines or shocks) from the initial condition intersect with one another. The coordinates of the four nodes serving as the end points of the three intervals \mathbf{e}_1 , \mathbf{e}_2 and \mathbf{e}_3 at time Δt can be determined as

$$\begin{aligned} x_1(\Delta t) &= x_r + q'_2(\rho_r)\Delta t, & x_2(\Delta t) &= x_r + q'_2(\rho_c)\Delta t, \\ x_3(\Delta t) &= x_r + q'_1(\rho_c)\Delta t, & x_4(\Delta t) &= x_r + q'_1(\bar{\rho}_l)\Delta t. \end{aligned}$$

The density at these end points at time Δt are given by

$$\rho(x_1(\Delta t), \Delta t) = \rho_r, \quad \rho(x_2(\Delta t), \Delta t) = \rho_c, \quad \rho(x_3(\Delta t), \Delta t) = \rho_c, \quad \rho(x_4(\Delta t), \Delta t) = \bar{\rho}_l$$

and the density is linear within each of the new intervals \mathbf{e}_i , $i = 1, 2, 3$. In particular, the density within \mathbf{e}_2 is a constant $\rho = \rho_c$.

2.3 Boundary conditions from the highway entrance

In this subsection we discuss the boundary condition at the left boundary $x = 0$, which is the highway entrance.

Looking at the solution (6)-(7), we can see that the general solution with a linear initial condition is not linear in t for fixed x , unless $\beta = 0$, in which case the solution is constant in t . Therefore, within our piecewise linear (in space) framework, we can only consider piecewise constant boundary conditions. A typical boundary condition at $x = 0$ is shown in Figure 5.

We now use the notation in the previous sections. The interface is at $x_r = \bar{x}_l = 0$, and the left density value ρ_r at $x = 0$ is given by the boundary condition. Otherwise, this is identical to the situation studied in the two previous subsections for an internal generalized Riemann problem. Again, we would need to consider the situation where ρ_r and the linear function in

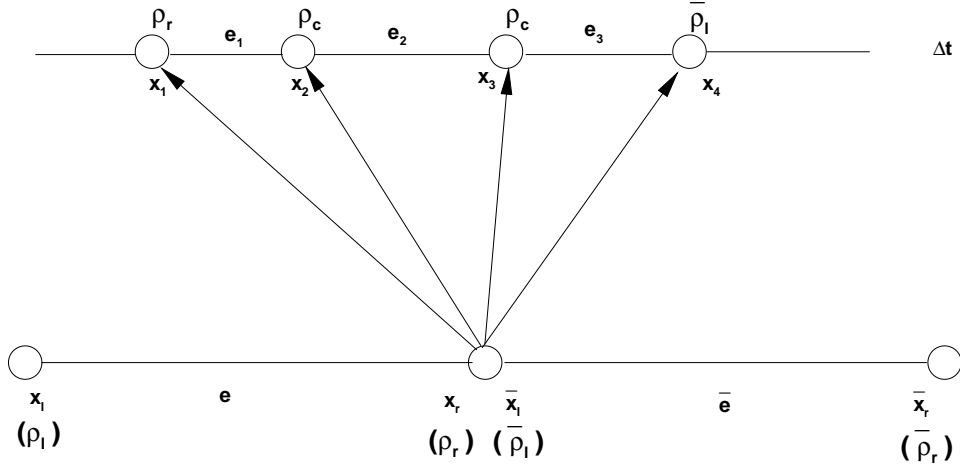


Figure 4: Propagation of a rarefaction wave from a nodal point.

the first interval with end values $\bar{\rho}_l$ and $\bar{\rho}_r$ belong to different regimes in (4), for otherwise the solution is the one obtained in (Wong and Wong, 2002b). If $\rho_r \leq \rho_c \leq \bar{\rho}_l$, a shock is generated. We consider only the situation that the shock moves to the right. Its location Δx after time Δt is given by (13), except that the left flux \hat{f}_l given by (8) is simplified to

$$\hat{f}_l = q_1(\rho_r) \Delta t$$

and the top flux \hat{f}_t given by (11) is simplified to

$$\hat{f}_t = \rho_r \Delta x.$$

Therefore, the coefficients in the quadratic equation (13) which determines the shock location

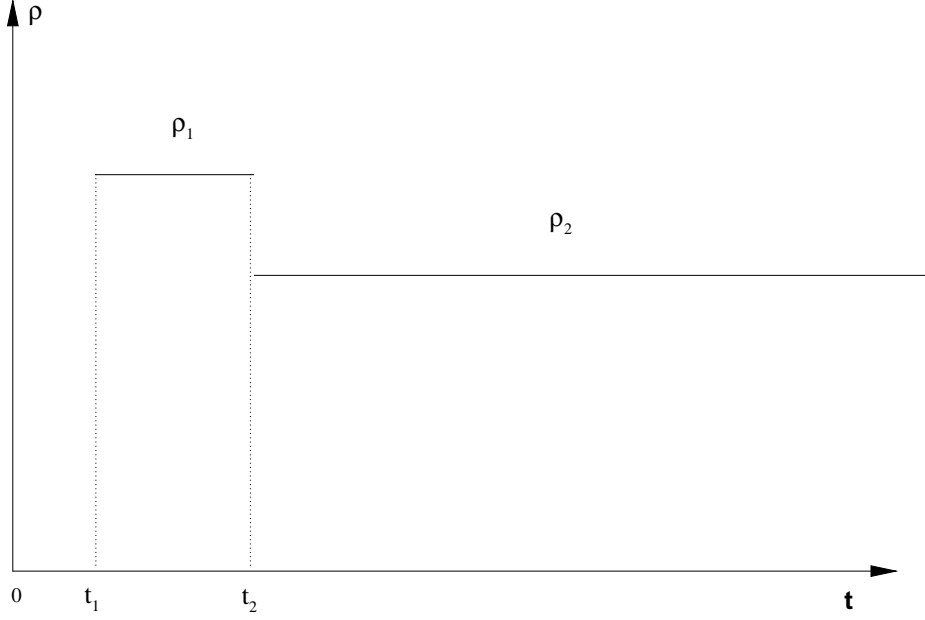


Figure 5: A typical boundary condition at the entrance $x = 0$.

Δx are simplified to

$$\begin{aligned}
 F_1(\Delta t) &= \bar{\rho}_r - \bar{\rho}_l \\
 F_2(\Delta t) &= 2[e_1(\bar{\rho}_l - \bar{\rho}_r)\Delta t + 2e_2\rho_r(\bar{\rho}_l - \bar{\rho}_r)\Delta t + (\rho_r - \bar{\rho}_l)(\bar{x}_l - \bar{x}_r)] \\
 F_3(\Delta t) &= -\Delta t\{[e_1^2 + 4(d_0 - e_0)e_2](\bar{\rho}_l - \bar{\rho}_r)\Delta t + 2(d_0 - e_0 - e_1\bar{\rho}_l - e_2\bar{\rho}_l^2)(\bar{x}_l - \bar{x}_r) \\
 &\quad + 2d_1\rho_r[2e_2(\bar{\rho}_l - \bar{\rho}_r)\Delta t + \bar{x}_l - \bar{x}_r] + 2d_2\rho_r^2[2e_2(\bar{\rho}_l - \bar{\rho}_r)\Delta t + \bar{x}_l - \bar{x}_r]\}.
 \end{aligned}$$

When $\rho_r \geq \rho_c \geq \bar{\rho}_l$, a rarefaction wave is formed. The formulas are the same as those given in Section 2.2.

2.4 Boundary conditions for the highway exit

In this subsection we discuss the boundary condition at the right boundary $x = x_{end}$, which is the highway exit.

We consider a typical exit setup with a traffic signal, which alternates between green and red lights. This is similar to the piecewise constant boundary condition considered for the entrance in the previous subsection. The constant values of the density ρ for the green and red lights are $\bar{\rho}_l = 0$ and $\bar{\rho}_l = \rho_{\max}$, respectively.

When $\bar{\rho}_l = \rho_{\max}$, corresponding to the situation of a red light, a left-moving shock is formed. We again only consider the situation $\rho_r \leq \rho_c \leq \bar{\rho}_l$, corresponding to the situation where the density at the left of x_{end} belongs to the regime of Flux I in (4). The value Δx determining the shock location $x_{end} + \Delta x$ after time Δt (recall that in this case Δx is negative) is given by (19), except that the right flux \hat{f}_r given by (16) is simplified to

$$\hat{f}_r = 0$$

and the top flux \hat{f}_t given by (18) is simplified to

$$\hat{f}_t = \rho_{\max} \Delta x.$$

Therefore, the coefficients in the quadratic equation (19) which determines the shock location $x_{end} + \Delta x$ are simplified to

$$\begin{aligned} \tilde{F}_1(\Delta t) &= \rho_l - \rho_r \\ \tilde{F}_2(\Delta t) &= -2[d_1(\rho_l - \rho_r)\Delta t + 2d_2\bar{\rho}_l(\rho_l - \rho_r)\Delta t + (\bar{\rho}_l - \rho_r)(x_l - x_r)] \\ \tilde{F}_3(\Delta t) &= \Delta t\{d_1^2(\rho_l - \rho_r)\Delta t + 2d_1\rho_r(-x_l + x_r) - 2\{-[e_0 + \bar{\rho}_l(e_1 + e_2\bar{\rho}_l)](x_l - x_r) \\ &\quad + d_0[2d_2(\rho_l - \rho_r)\Delta t + x_l - x_r] + d_2[-2e_2\rho_l\bar{\rho}_l^2\Delta t + 2e_2\bar{\rho}_l^2\rho_r\Delta t + 2e_0(\rho_r - \rho_l)\Delta t \\ &\quad + 2e_1\bar{\rho}_l(\rho_r - \rho_l)\Delta t + \rho_r^2x_l - \rho_r^2x_r]\}\} \end{aligned}$$

When $\bar{\rho}_l = 0$, corresponding to the situation of a green light, a rarefaction wave is formed. The formulas are the same as those given in Section 2.2.

3 Solution procedure

In this section we summarize the solution procedure, concentrating on the discussion of finding the earliest time when the waves (characteristic lines or shocks) from the previous

initial condition intersect with one another and hence the construction of the entropy solution must be restarted based on a new piecewise linear initial data.

Recall our assumption, as stated in Section 2, that the x -axis is divided into a number of intervals, within each of them the initial density is given by a linear function $\rho(x, 0) = \alpha + \beta x$ which is completely contained in one of the regimes $\rho \leq \rho_c$ or $\rho \geq \rho_c$. We consider several cases of wave interactions separately below, and then take the smallest time from these cases, which will serve as the time to restart the solution procedure with a new piecewise linear initial data. The cases being considered are: natural break time for each individual linear piece, and the interaction between waves from two adjacent nodes (including the boundary nodes). For the latter case, we also distinguish between the situation of the two adjacent nodes corresponding to a shock and a rarefaction wave respectively, and the situation of the two adjacent nodes both corresponding to shocks. Notice that the situation of the two adjacent nodes both corresponding to rarefaction waves are included in the case of natural break time for the individual linear piece between the two nodes.

Once the smallest time of wave interactions is found, the density function is obtained at this time using the formulas in Section 2 as a new piecewise linear function, and the procedure is repeated, until the final desired time is reached.

3.1 Natural break time for each individual linear piece

For an element \mathbf{e} in which the initial linear density profile is an increasing function, the natural break time, see Figure 6, can be determined by the following formula (Whitham, 1974):

$$\tau_e = -\frac{1}{q''(\rho) \frac{\partial \rho}{\partial x}}$$

Notice that under our assumption (concave quadratic flux q and increasing linear density ρ) the denomination is a negative constant, hence τ_e is a positive constant. Indeed, if the interval $\mathbf{e} = (x_l, x_r)$ and the initial condition density values at the interval boundaries are $\rho_l = \rho(x_l^+, 0)$ and $\rho_r = \rho(x_r^-, 0)$, see Figure 6, and assuming that the flux function in the

element \mathbf{e} is:

$$q(\rho) = a_0 + a_1 \rho + a_2 \rho^2$$

then

$$\tau_e = \begin{cases} \frac{x_r - x_l}{2a_2(\rho_l - \rho_r)} & \rho_r > \rho_l \\ \infty & \text{otherwise} \end{cases} \quad (21)$$

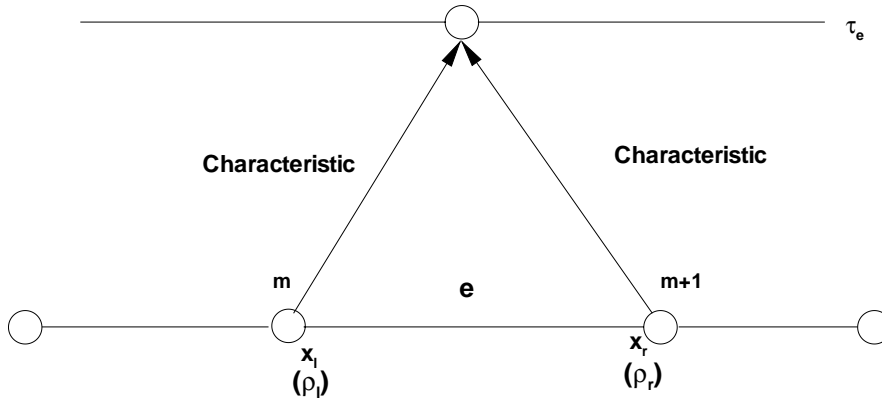


Figure 6: Natural break for an increasing linear profile.

3.2 A shock intersecting with its adjacent characteristic line

We consider the situation that a shock from the element boundary $x_r = \bar{x}_l$ intersects with the characteristic line from the right boundary \bar{x}_r of the element $\bar{\mathbf{e}}$, see Figure 7.

Assuming the flux function in the element \mathbf{e} is

$$q_1(\rho) = d_0 + d_1 \rho + d_2 \rho^2$$

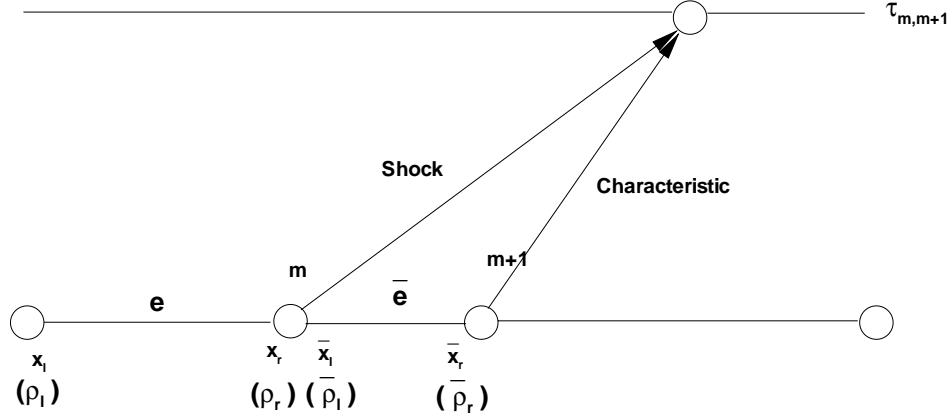


Figure 7: A shock intersecting with its right neighbor's characteristic line

and the flux function in the element \bar{e} is

$$q_2(\rho) = e_0 + e_1 \rho + e_2 \rho^2,$$

by substituting the straight line function of the characteristic line from the node \bar{x}_r into the shock location trajectory (13) for the shock from the node $x_r = \bar{x}_l$, we obtain a cubic equation for the intersecting time t :

$$T_1 t^3 + T_2 t^2 + T_3 t + T_4 = 0 \quad (22)$$

where, with $\delta_1 = \bar{x}_r - \bar{x}_l$, $\delta_2 = x_r - x_l$, we have

$$T_1 = -2e_2(\rho_l - \rho_r)(\bar{\rho}_l - \bar{\rho}_r)[d_1^2 - 4d_0d_2 + 4d_2e_0 + e_1^2 + 4e_1e_2\bar{\rho}_r - 4d_2e_2\bar{\rho}_r^2 + 4e_2^2\bar{\rho}_r^2 - 2d_1(e_1 + 2e_2\bar{\rho}_r)]$$

$$\begin{aligned}
T_2 &= (d_1^2 + e_1^2)(\rho_l - \rho_r)\delta_1 - 4e_1e_2\{\rho_l(\bar{\rho}_l - 2\bar{\rho}_r)\delta_1 + \rho_r[-\bar{\rho}_l(\delta_1 + \delta_2) + \bar{\rho}_r(2\delta_1 + \delta_2)]\} \\
&\quad 2d_1\{-e_1(\rho_l - \rho_r)\delta_1 + 2e_2\{\rho_l(\bar{\rho}_l - 2\bar{\rho}_r)\delta_1 + \rho_r[-\bar{\rho}_l(\delta_1 + \delta_2) + \bar{\rho}_r(2\delta_1 + \delta_2)]\}\} \\
&\quad + 4\{e_2\{-(d_0 - e_0)(\bar{\rho}_l - \bar{\rho}_r)\delta_2 + e_2\bar{\rho}_r\{\rho_l(-2\bar{\rho}_l + 3\bar{\rho}_r)\delta_1 + \bar{\rho}_r[-\rho_r(3\delta_1 + 2\delta_2) + \bar{\rho}_r\delta_2] \\
&\quad + \bar{\rho}_l[-\bar{\rho}_r\delta_2 + 2\rho_r(\delta_1 + \delta_2)]\}\} + d_2\{-(d_0 - e_0)(\rho_l - \rho_r)\delta_1 + e_2\{\rho_l(\bar{\rho}_l^2 - 2\bar{\rho}_r^2)\delta_1 + \\
&\quad \rho_r[-\bar{\rho}_l^2\delta_1 - \bar{\rho}_l\rho_r\delta_2 + \bar{\rho}_r(2\bar{\rho}_r\delta_1 + \rho_r\delta_2)]\}\}\} \\
T_3 &= 2\{d_2[-\rho_l\delta_1^2(\bar{\rho}_l + \bar{\rho}_r) + \rho_r(\bar{\rho}_l\delta_1^2 + \bar{\rho}_r\delta_1^2 + \rho_r\delta_1\delta_2)] - \delta_1\{-(d_0 - e_0)\delta_2 + d_1[\rho_l\delta_1 - \rho_r(\delta_1 + \delta_2)] \\
&\quad e_1[-\rho_l\delta_1 + \rho_r(\delta_1 + \delta_2)]\} + e_2\{\rho_l\delta_1^2(-\bar{\rho}_l + 3\bar{\rho}_r) - \bar{\rho}_l^2\delta_1\delta_2 + \bar{\rho}_l\rho_r\delta_1(\delta_1 + 2\delta_2) \\
&\quad - \bar{\rho}_r[-2\bar{\rho}_r\delta_1\delta_2 + \rho_r(3\delta_1^2 + 4\delta_1\delta_2)]\}\} \\
T_4 &= \delta_1^2[(\bar{\rho}_l + \bar{\rho}_r)\delta_2 + \rho_l\delta_1 - \rho_r(\delta_1 + 2\delta_2)]
\end{aligned}$$

We can then determine the earliest intersection point of the shock and the characteristic line by finding the smallest positive root of equation (22). As this is a cubic equation and exact root formulas exist, such a root can be found readily.

A symmetric situation is when a shock from the element boundary $x_r = \bar{x}_r$ intersects with the characteristic line from the left boundary x_l of the element \mathbf{e} , see Figure 8.

The procedure to obtain the intersecting time is similar. We have the cubic equation

$$\tilde{T}_1 t^3 + \tilde{T}_2 t^2 + \tilde{T}_3 t + \tilde{T}_4 = 0 \quad (23)$$

where, with $\delta_1 = x_r - x_l$, $\delta_2 = \bar{x}_r - \bar{x}_l$, we have

$$\begin{aligned}
\tilde{T}_1 &= 2d_2[d_1^2 - 2d_1e_1 + e_1^2 + 4e_2(d_0 - e_0) + 4d_2\rho_l(d_1 - e_1) + 4d_2\rho_l^2(d_2 - e_2)](\rho_l - \rho_r)(\bar{\rho}_l - \bar{\rho}_r) \\
\tilde{T}_2 &= -d_1^2(\bar{\rho}_l - \bar{\rho}_r)\delta_1 - [e_1^2 + 4(d_0 - e_0)e_2](\bar{\rho}_l - \bar{\rho}_r)\delta_1 - 4d_2\rho_l\{-\rho_l^2\delta_2 + 2\rho_r[\bar{\rho}_r\delta_1 - \bar{\rho}_l(\delta_1 + \delta_2)] \\
&\quad + \rho_l[-3\bar{\rho}_r\delta_1 + \rho_r\delta_2 + \bar{\rho}_l(3\delta_1 + 2\delta_2)]\} - 2d_1\{-e_1(\bar{\rho}_l - \bar{\rho}_r)\delta_1 + 2d_2\{\rho_r[\bar{\rho}_r\delta_1 - \bar{\rho}_l(\delta_1 + \delta_2)] \\
&\quad + \rho_l[-2\bar{\rho}_r\delta_1 + \bar{\rho}_l(2\delta_1 + \delta_2)]\}\} + 4d_2\{-(d_0 - e_0)(\rho_l - \rho_r)\delta_2 + e_2[2\rho_l^2(\bar{\rho}_l - \bar{\rho}_r)\delta_1 + \rho_l\bar{\rho}_l^2\delta_2 \\
&\quad + \rho_r(-\bar{\rho}_l\rho_r\delta_1 + \rho_r\bar{\rho}_r\delta_1 - \bar{\rho}_l^2\delta_2)] + e_1\{\rho_r[\bar{\rho}_r\delta_1 - \bar{\rho}_l(\delta_1 + \delta_2)] + \rho_l[-2\bar{\rho}_r\delta_1 + \bar{\rho}_l(2\delta_1 + \delta_2)]\}\}
\end{aligned}$$

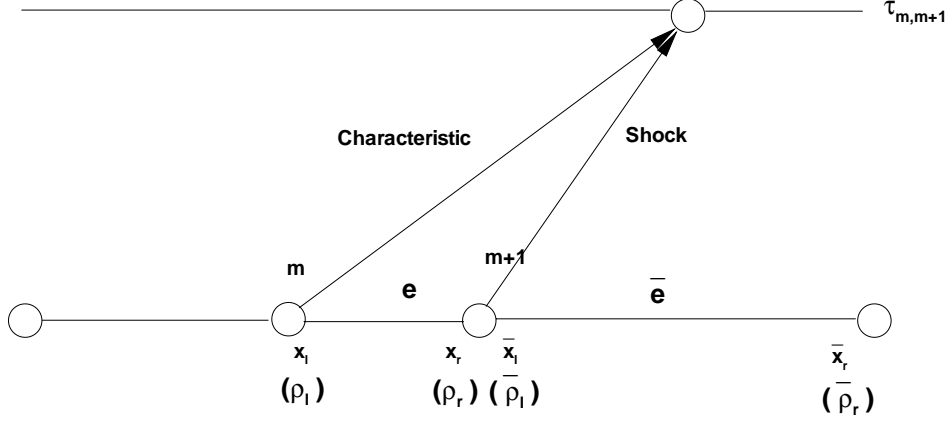


Figure 8: A shock intersecting with its left neighbor's characteristic line

$$\begin{aligned}
\tilde{T}_3 &= 2\{e_2\{[-\bar{\rho}_l\rho_r + \rho_r\bar{\rho}_r + \rho_l(-\bar{\rho}_l + \bar{\rho}_r)]\delta_1^2 - \bar{\rho}_l^2\delta_1\delta_2\} + \delta_1\{(d_0 - e_0)\delta_2 \\
&\quad + [\bar{\rho}_r\delta_1 - \bar{\rho}_l(\delta_1 + \delta_2)](e_1 - d_1)\} \\
&\quad + d_2\{-\rho_l^2\delta_1\delta_2 + \rho_r[\bar{\rho}_r\delta_1^2 + \rho_r\delta_1\delta_2 - \bar{\rho}_l\delta_1(\delta_1 + 2\delta_2)] + \rho_l[-3\bar{\rho}_r\delta_1^2 + \bar{\rho}_l(3\delta_1^2 + 4\delta_1\delta_2)]\}\} \\
\tilde{T}_4 &= \delta_1^2[\bar{\rho}_r\delta_1 + (\rho_l + \rho_r)\delta_2 - \bar{\rho}_l(\delta_1 + 2\delta_2)]
\end{aligned}$$

3.3 Two intersecting adjacent shocks

We now consider the situation that two adjacent nodes x_m and x_{m+1} correspond to two shocks which will intersect at time Δt , see Figure 9. This is the most difficult case since no closed form formula exists for the intersecting time Δt . We will therefore resort to a nonlinear equation solver such as the Newton's method.

We assume that the shock location of the shock from the node x_m at time Δt is $x_m + \Delta x_m$ and denote $G_m(\Delta t) = \Delta x_m$. Likewise, the shock location of the shock from the node x_{m+1}

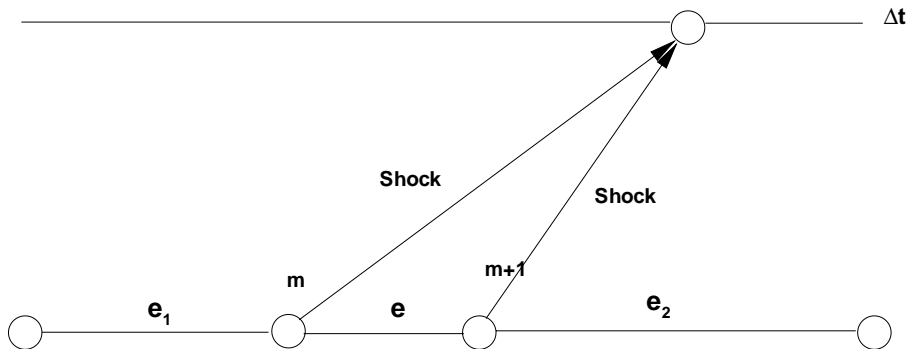


Figure 9: Two intersecting adjacent shocks.

at time Δt is $x_{m+1} + \Delta x_{m+1}$ and we denote $G_{m+1}(\Delta t) = \Delta x_{m+1}$. The displacements $G_m(\Delta t)$ and $G_{m+1}(\Delta t)$ are determined by (13) or (19). Therefore, we can define the function

$$S(\Delta t) = x_{m+1} - x_m + G_{m+1}(\Delta t) - G_m(\Delta t) \quad (24)$$

which measures the distance between the two shocks. Clearly, $S(0) = x_{m+1} - x_m > 0$, and we would like to find the root of $S(\Delta t)$, which corresponds to the time that the two shocks intersect. As for each *fixed* Δt , $S(\Delta t)$ and $S'(\Delta t)$ can both be readily computed, we can easily set up a Newton iteration to solve for the root of $S(\Delta t)$ with $\Delta t = 0$ as the initial guess. In the Appendix, we will show the uniqueness of the intersecting point of the two shock curves before the natural break time of the element in between, if they do intersect. Therefore, $S(\Delta t)$ has at most one zero before the natural break time of the element in between, which facilitates the convergence of the Newton iteration procedure.

4 Numerical examples

In this section we provide three numerical examples to illustrate the explicit formulas for the entropy solutions obtained in the previous sections. The flow-density relationship is given by (3)-(4), with

$$q(\rho) = \begin{cases} -0.4\rho^2 + 100\rho, & 0 \leq \rho \leq 50 \\ -0.1\rho^2 + 15\rho + 3500, & 50 \leq \rho \leq 100 \\ -0.024\rho^2 - 5.2\rho + 4760, & 100 \leq \rho \leq 350 \end{cases}$$

see Figure 10.

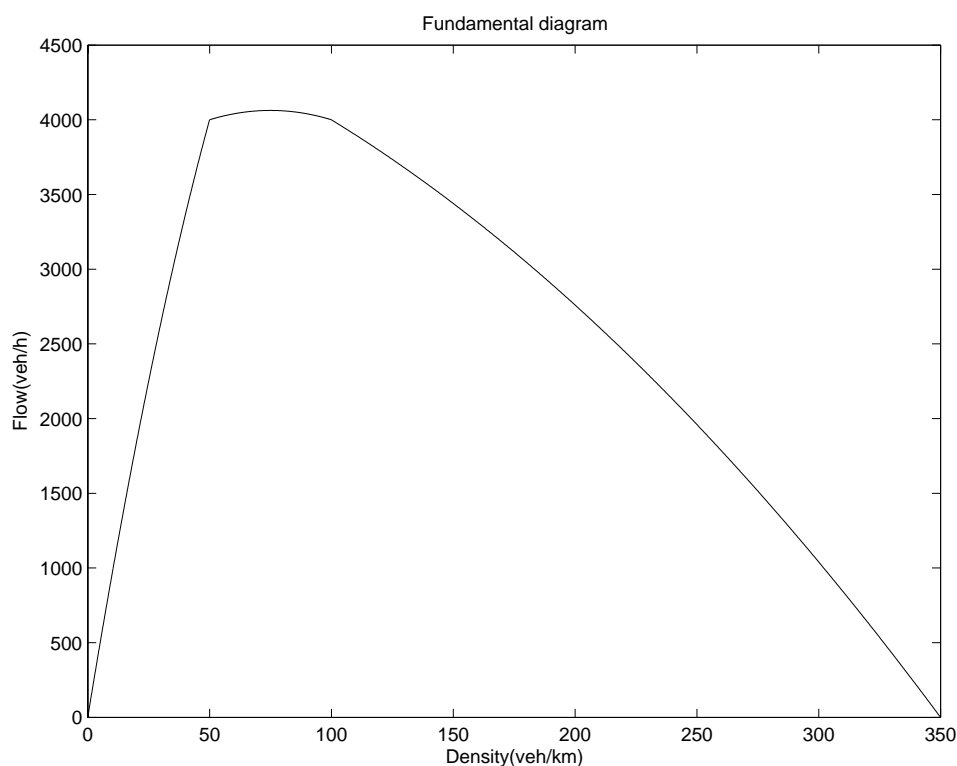


Figure 10: Flow-density relationship used in the numerical examples.

We also use the fifth order finite difference WENO scheme (Jiang and Shu, 1996; Zhang et al., 2003) to compute the solution and make a comparison. The purpose of this comparison is to validate the computation of WENO schemes against the presumably exact entropy solutions obtained by the procedure in this paper.

Example 1. Consider a homogeneous highway with a length of 2 km. Due to a certain

incident on the road, an initial density distribution with a peak of 150 veh/km is formed as shown in Figure 11. Assume that the entrance of the highway is blocked and no traffic is allowed to enter from the upstream end. The exact solution of this problem can be worked out using the procedure in this paper, shown as solid lines in Figure 12, in comparison with the numerical solution obtained by the WENO scheme using $N = 200$ uniform grid points, shown as circles. We can see that the two results agree quite well.

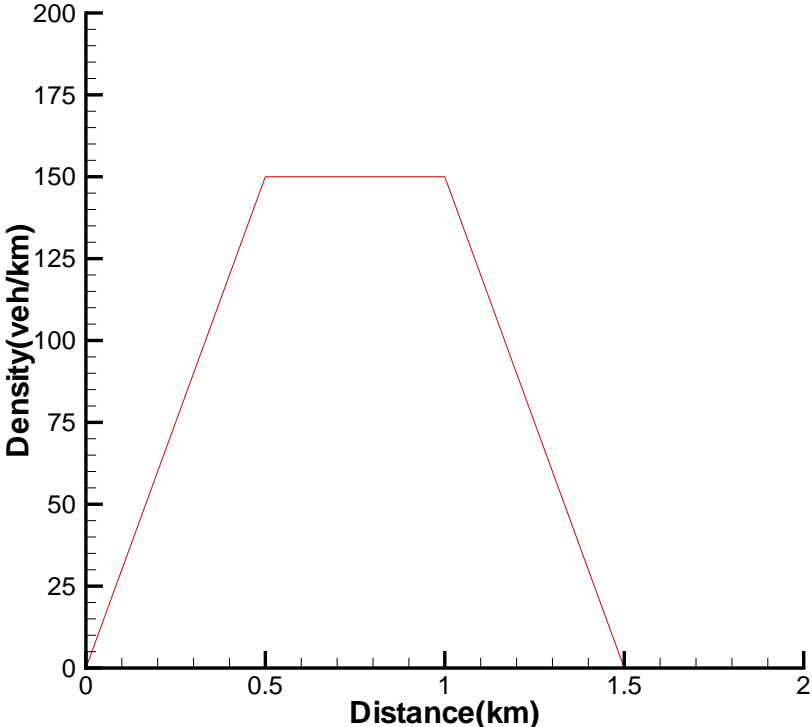


Figure 11: The initial density profile for Example 1.

In order to demonstrate the performance of the solution procedure derived in this paper, we show in Figure 13 the space-time diagram of all waves (shocks and rarefaction waves) involved in the evolution process for Example 1 until $t = 3.0$ min. The relevant breaking points and density values at nodes are also shown in Table 1. We can see that the procedure works well for this example with relatively few restarts to reach the target time $t = 3.0$ min.

Table 1: Breaking points and density values at nodes for the evolution process for Example 1 until $t = 3.0$ min.

Time (min)	Element	x_l (km)	x_r (km)	ρ_l (veh/km)	ρ_r (veh/km)
$t_0 = 0$	1	0.000	0.167	0.0	50.0
	2	0.167	0.333	50.0	100.0
	3	0.333	0.500	100.0	150.0
	4	0.500	1.000	150.0	150.0
	5	1.000	1.167	150.0	100.0
	6	1.167	1.333	100.0	50.0
	7	1.333	1.500	50.0	0.0
	8	1.500	2.000	0.0	0.0
$t_1 = 0.162$	1	0.000	0.271	0.0	0.0
	2	0.271	0.313	82.4	97.7
	3	0.313	0.466	102.2	150.0
	4	0.466	0.966	150.0	150.0
	5	0.966	1.140	150.0	100.0
	6	1.140	1.153	100.0	100.0
	7	1.153	1.347	100.0	50.0
	8	1.347	1.496	50.0	50.0
	9	1.496	1.771	50.0	0.0
	10	1.771	2.000	0.0	0.0
$t_2 = 0.211$	1	0.000	0.307	0.0	0.0
	2	0.307	0.456	102.9	150.0
	3	0.456	0.956	150.0	150.0
	4	0.956	1.131	150.0	100.0
	5	1.131	1.149	100.0	100.0
	6	1.149	1.351	100.0	50.0
	7	1.351	1.545	50.0	50.0
	8	1.545	1.852	50.0	0.0
	9	1.852	2.000	0.0	0.0
$t_3 = 0.300$	1	0.000	0.358	0.0	0.0
	2	0.358	0.438	124.0	150.0
	3	0.438	0.938	150.0	150.0
	4	0.938	1.117	150.0	100.0
	5	1.117	1.142	100.0	100.0
	6	1.142	1.358	100.0	50.0
	7	1.358	1.633	50.0	50.0
	8	1.633	2.000	50.0	0.0

Table 1: (continued)

$t_4 = 0.425$	1	0.000	0.412	0.0	0.0
	2	0.412	0.912	150.0	150.0
	3	0.912	1.096	150.0	100.0
	4	1.096	1.131	100.0	100.0
	5	1.131	1.369	100.0	50.0
	6	1.369	1.758	50.0	50.0
	7	1.758	2.000	50.0	23.1
$t_5 = 0.667$	1	0.000	0.505	0.0	0.0
	2	0.505	0.862	150.0	150.0
	3	0.862	1.056	150.0	100.0
	4	1.056	1.111	100.0	100.0
	5	1.111	1.389	100.0	50.0
	6	1.389	2.000	50.0	50.0
$t_6 = 1.274$	1	0.000	0.737	0.0	0.0
	2	0.737	0.954	150.0	100.0
	3	0.954	1.061	100.0	100.0
	4	1.061	1.439	100.0	50.0
	5	1.439	2.000	50.0	50.0
$t_7 = 1.600$	1	0.000	0.900	0.0	0.0
	2	0.900	1.033	100.0	100.0
	3	1.033	1.467	100.0	50.0
	4	1.467	2.000	50.0	50.0
$t_8 = 1.778$	1	0.000	1.019	0.0	0.0
	2	1.019	1.481	100.0	50.0
	3	1.481	2.000	50.0	50.0
$t_9 = 2.333$	1	0.000	1.528	0.0	0.0
	2	1.528	2.000	50.0	50.0
$t_{10} = 2.711$	1	0.000	2.000	0.0	0.0
$t_{11} = 3.000$	1	0.000	2.000	0.0	0.0

Example 2. We consider a long homogeneous freeway of length 20 km. The entrance density is 50 veh/km. Due to an incident near the downstream end of the freeway, the traffic density profile shown in Figure 14 is formed in which a jam-packed condition of 5 km long occurs from 10 to 15 km measured from the upstream entrance of the freeway. In order to release the traffic jam condition downstream, the authority blocks the freeway entrance for 10 min, after which traffic is released again from the freeway entrance at the capacity density of 75 veh/km. After 20 min, the entrance flow returns back to normal with a density of 50 veh/h. The variation of traffic density at the upstream entrance of the freeway is illustrated in Figure 15. The period of analysis is 2 hours.

The exact solution of this problem is worked out using the procedure in this paper, shown as solid lines in Figure 16, in comparison with the numerical solution obtained by the WENO scheme using $N = 200$ uniform grid points, shown as circles. We can again see that the two results agree quite well.

Again, in order to demonstrate the performance of the solution procedure derived in this paper, we show in Figure 17 the space-time diagram of all waves (shocks and rarefaction waves) involved in the evolution process for Example 2 until $t = 120$ min. The relevant breaking points and density values at nodes are also shown in Table 2. We can see that the procedure works well for this example with relatively few restarts to reach the target time $t = 120$ min.

Example 3. This example has the same initial condition and entrance boundary condition as those in Example 2. However, at the exit boundary, a traffic signal is installed, with a repeated pattern of 2 minutes green light followed by 1 minute red light.

As before, the exact solution of this problem is worked out using the procedure in this paper, shown as solid lines in Figure 18, in comparison with the numerical solution obtained by the WENO scheme using $N = 400$ uniform grid points, shown as circles. We see once again that the two results agree quite well.

Table 2: Breaking points and density values at nodes for the evolution process for Example 2 until $t = 120$ min.

Time (min)	Element	x_l (km)	x_r (km)	ρ_l (veh/km)	ρ_r (veh/km)
$t_0 = 0$	1	0.000	10.000	50.0	50.0
	2	10.000	15.000	350.0	350.0
	3	15.000	18.571	350.0	100.0
	4	18.571	19.286	100.0	50.0
	5	19.286	20.000	50.0	0.0
$t_1 = 0.714$	1	0.000	0.952	0.0	0.0
	2	0.952	9.841	50.0	50.0
	3	9.841	14.738	350.0	350.0
	4	14.738	18.452	350.0	100.0
	5	18.452	18.512	100.0	100.0
	6	18.512	19.345	100.0	50.0
	7	19.345	20.000	50.0	50.0
$t_2 = 6.429$	1	0.000	8.571	0.0	0.0
	2	8.571	12.643	350.0	350.0
	3	12.643	17.500	350.0	100.0
	4	17.500	18.036	100.0	100.0
	5	18.036	19.821	100.0	50.0
	6	19.821	20.000	50.0	50.0
$t_3 = 8.571$	1	0.000	8.571	0.0	0.0
	2	8.571	11.857	350.0	350.0
	3	11.857	17.143	350.0	100.0
	4	17.143	17.857	100.0	100.0
	5	17.857	20.000	100.0	50.0
$t_4 = 10.000$	1	0.000	8.571	0.0	0.0
	2	8.571	11.333	350.0	350.0
	3	11.333	16.905	350.0	100.0
	4	16.905	17.738	100.0	100.0
	5	17.738	20.000	100.0	52.5
$t_5 = 15.143$	1	0.00	0.429	75.0	50.0
	2	0.429	5.143	50.0	50.0
	3	5.143	8.571	50.0	0.0
	4	8.571	9.448	350.0	350.0
	5	9.448	16.048	350.0	100.0
	6	16.048	17.310	100.0	100.0
	7	17.310	20.000	100.0	58.5

Table 2: (continued)

$t_6 = 18.182$	1	0.000	0.682	75.0	50.0
	2	0.682	8.182	50.0	50.0
	3	8.182	8.333	350.0	350.0
	4	8.333	15.541	350.0	100.0
	5	15.541	17.056	100.0	100.0
	6	17.056	20.000	100.0	60.7
$t_7 = 19.231$	1	0.000	0.769	75.0	50.0
	2	0.769	7.949	50.0	50.0
	3	7.949	15.366	350.0	100.0
	4	15.366	16.969	100.0	100.0
	5	16.969	20.000	100.0	61.3
$t_8 = 30.000$	1	0.000	1.667	75.0	50.0
	2	1.667	5.678	50.0	50.0
	3	5.678	13.571	306.2	100.0
	4	13.571	16.071	100.0	100.0
	5	16.071	20.000	100.0	65.6
$t_9 = 44.742$	1	0.000	0.698	50.0	50.0
	2	0.698	2.895	69.0	50.0
	3	2.895	11.115	264.1	100.0
	4	11.115	14.843	100.0	100.0
	5	14.843	20.000	100.0	68.4
$t_{10} = 54.000$	1	0.000	1.195	50.0	50.0
	2	1.195	9.571	245.7	100.0
	3	9.571	14.071	100.0	100.0
	4	14.071	20.000	100.0	69.5
$t_{11} = 61.319$	1	0.000	8.352	231.9	100.0
	2	8.352	13.462	100.0	100.0
	3	13.462	20.000	100.0	70.1
$t_{12} = 111.429$	1	0.000	9.286	100.0	100.0
	2	9.286	20.000	100.0	72.2
$t_{13} = 120.000$	1	0.000	8.571	100.0	100.0
	2	8.571	20.000	100.0	72.4

Table 3: CPU time comparison between the solution procedure in this paper and the fifth order WENO scheme.

Example #	Analytical (sec)	WENO (sec)	N	ending time t (min)
Example 1	1.669×10^{-3}	0.3484	200	3
Example 2	2.675×10^{-3}	0.4609	200	120
Example 3	7.933×10^{-2}	2.045	400	120

Finally, in Table 3 we compare the CPU time used by the procedure in this paper and by the fifth order WENO scheme with an appropriate number of uniform grid points to achieve a comparable accuracy, for the three examples shown above. We can see clearly that the exact solution procedure developed in this paper is much less CPU time intensive than the finite difference WENO method.

5 Conclusions

We have developed in this paper a procedure to explicitly compute the entropy solution for a Lighthill-Whitham-Richards traffic flow model with with a flow-density relationship which is piecewise quadratic, continuous, concave, but not differentiable at the junction points, and with piecewise linear initial condition and piecewise constant boundary conditions. The procedure usually involves very few restarts and hence rapid computation for realistic traffic flow situations, using very small CPU time comparing with a high order finite difference WENO scheme. Three representative numerical examples, involving various initial and boundary conditions including that for traffic control signals, are used to demonstrate the efficiency and effectiveness of this solution procedure. The solutions obtained agree very well with those obtained by the finite difference WENO scheme which uses much more CPU time. In future work we will attempt to remove the condition of continuity for the flow-density relationship in order to better model certain realistic traffic flows such as the famous λ -waves.

6 Acknowledgements

The research of the first author was partially supported by a grant from the Research Grants Council of the Hong Kong Special Administrative Region, China (HKU7031/02E), when he was a visiting student at the Department of Civil Engineering of the University of Hong Kong. The work of the second author was partially supported by grants from the Research Grants Council of the Hong Kong Special Administrative Region, China (HKU7031/02E and HKU7187/05E). The research of the third author was partially supported by the Chinese Academy of Sciences grant 2004-1-8. The research of the fourth author was partially supported by the Chinese Academy of Sciences while he was visiting the University of Science and Technology of China (grant 2004-1-8) and the Institute of Computational Mathematics and Scientific / Engineering Computing. Additional support was provided by ARO grant W911NF-04-1-0291, NSF grant DMS-0510345 and AFOSR grant FA9550-05-1-0123.

References

- [1] Ansorge, R., 1990. What does the entropy condition mean in traffic flow theory. *Transportation Research Part B*, 24 (2), 133-143.
- [2] Biham, O., Middleton, A.A., Levine, D., 1992. Self-organization and a dynamic transition in traffic-flow models. *Physical Review A*, 46 (10), R6124-R6127.
- [3] Cuesta, J.A., Martinez, F.C., Molera, J.M., Sanchez, A. 1993. Phase-transitions in 2-dimensional traffic-flow models. *Physical Review E*, 48 (6), R4175-R4178.
- [4] Dafermos, C.M., 1972. Polygonal approximations of solutions of initial value-problem for a conservation law. *Journal of Mathematical Analysis and Applications*, 38 (1), 33-41.
- [5] Daganzo, C.F., 1994. The cell transmission model - a dynamic representation of highway traffic consistent with the hydrodynamic theory. *Transportation Research Part B*, 28 (4), 269-287.

- [6] Daganzo, C.F., 1995. A finite difference approximation of the kinematic wave model of traffic flow. *Transportation Research Part B*, 29 (4), 261-276.
- [7] Dick, A.C., 1966. Speed/flow relationships within an urban area. *Traffic Engineering and Control*, 8 (6), 393-396.
- [8] Edie, L.C., 1961. Car-following and steady-state theory for noncongested traffic. *Operations Research*, 9 (1), 66-76.
- [9] Greenshields, B.D., 1934. A study of traffic capacity. *Proceedings of Highway Research Board*, 14, 448-477.
- [10] Haberman, R., 1977. *Mathematical Models: Mechanical Vibrations, Population Dynamics, and Traffic Flow*, Prentice-Hall Inc., Englewood Cliffs, New Jersey.
- [11] Helbing, D., 1996. Gas-kinetic derivation of Navier-Stokes-like traffic equations. *Physical Review E*, 53 (3), 2366-2381.
- [12] Hoogendoorn, S.P., Bovy, P.H.L., 2000. Continuum modeling of multiclass traffic flow. *Transportation Research Part B*, 34 (2), 123-146.
- [13] Jiang, G.S., Shu, C.W., 1996. Efficient implementation of weighted ENO schemes. *Journal of Computational Physics*, 126 (1), 202-228.
- [14] Kerner, B.S., Konhauser, P., 1994. Structure and parameters of clusters in traffic flow. *Physical Review E*, 50 (1), 54-83.
- [15] Krauss, S., Wagner, P., Gawron, C., 1997. Metastable states in a microscopic model of traffic flow. *Physical Review E*, 55 (5), 5597-5602.
- [16] Lax, P., 1973. *Hyperbolic Systems of Conservation Laws and the Mathematical Theory of Shock Waves*, SIAM Regional Conference Series in Applied Mathematics, # 11, SIAM, Philadelphia.

- [17] Lebacque, J.P., 1996. The Godunov scheme and what it means for first order traffic flow models. In J.B. Lesort (ed), Proceedings of the 13th International Symposium on Transportation and Traffic Theory, Elsevier Science Ltd, Lyon, France, pp. 647-677.
- [18] LeVeque, R.J., 1992. Numerical Methods for Conservation Laws, Lecture in Mathematics, ETH Zurich, Birkhauser Verlag, Basel, Switzerland.
- [19] Lighthill, M.J., Whitham, G.B., 1955. On kinetic wave II: a theory of traffic flow on crowded roads. Proceedings of the Royal Society of London, Series A, 229 (1178), 317-345.
- [20] May, A.D., Keller, H.E.M., 1968. Evaluation of single and multi-regime traffic flow models. In W. Leutzbach and P. Baron (eds.), Proceedings of the 4th International Symposium on Theory of Traffic Flow, Karlsruhe, Germany.
- [21] Michalopoulos, P.G., Beskos, D.E., Lin, J.K., 1984. Analysis of interrupted traffic flow by finite-difference methods. Transportation Research Part B, 18 (4-5), 409-421.
- [22] Nagatani, T., 1993. Jamming transition in the traffic-flow model with 2-level crossings. Physical Review E, 48 (5), 3290-3294.
- [23] Nagel, K., Schreckenberg, M., 1992. A cellular automaton model for freeway traffic. Journal of Physique I, 2 (12), 2221-2229.
- [24] Nelson, P., Sopasakis, A., 1998. The Prigogine-Herman kinetic model predicts widely scattered traffic flow data at high concentrations. Transportation Research Part B, 32 (8), 589-604.
- [25] Newell, G.F., 1993. A simplified theory of kinematic waves in highway traffic, 1. general-theory. Transportation Research Part B, 27 (4), 281-287.

- [26] Pavieri-Fontana, S.L., 1975. Boltzmann-like treatments for traffic flow - critical review of basic model and an alternative proposal for dilute traffic analysis. *Transportation Research*, 9 (4), 225-235.
- [27] Payne, H.J., 1979. FREFLOW: a macroscopic simulation model of freeway traffic. *Transportation Research Record*, 722, 68-77.
- [28] Prigogine, I., Herman, R., 1971. *Kinetic Theory of Vehicular Traffic*, American Elsevier, New York.
- [29] Richards, P.I., 1956. Shock waves on the highway. *Operations Research*, 4 (1), 42-51.
- [30] Underwood, R.T., 1961. *Speed, volume and density relationships. Quality and Theory of Traffic Flow*, Bureau of Highway Traffic, Yale University, New Haven, CT.
- [31] Velan, S., Florian, M., 2002. A note on the entropy solutions of the hydrodynamic model of traffic flow. *Transportation Science*, 36 (4), 435-446.
- [32] Whitham, G.B., 1974. *Linear and Nonlinear Waves*, John Wiley & Sons, New York, USA.
- [33] Wong, G.C.K., Wong, S.C., 2002a. A multi-class traffic flow model - an extension of LWR model with heterogeneous drivers. *Transportation Research Part A*, 36 (9), 827-841.
- [34] Wong, S.C., Wong, G.C.K., 2002b. An analytical shock-fitting algorithm for LWR kinematic wave model embedded with linear speed-density relationship. *Transportation Research Part B*, 36 (8), 683-706.
- [35] Zhang, H.M., 1998. A theory of nonequilibrium traffic flow. *Transportation Research Part B*, 32 (7), 485-498.

- [36] Zhang, M., Shu, C.W., Wong, G.C.K., Wong, S.C., 2003. A weighted essentially non-oscillatory numerical scheme for a multi-class Lighthill-Whitham-Richards traffic flow model. *Journal of Computational Physics*, 191 (2), 639-659.

A Appendix

In this Appendix we study in more detail the situation discussed in Section 3.3, that two adjacent nodes correspond to two shocks which will intersect. Referring to Figure 19, we assume that two shocks $S_1(t)$ and $S_2(t)$, starting from the two adjacent nodes \bar{x}_l and \bar{x}_r , intersect first at time t^* . The inner element \mathbf{e} has two edge densities $\bar{\rho}_l$ and $\bar{\rho}_r$ at the foot of the shocks $S_1(0)$ and $S_2(0)$. We further assume that the intersecting time t^* is before the natural break time of the element \mathbf{e} given by (21); otherwise, we do not need to be concerned with the intersection time of the two shocks anyway because the solution procedure has already been restarted before the two shocks have the chance to intersect.

The shock curves $S_1(t)$ and $S_2(t)$, considered individually, may certainly be defined beyond $t = t^*$. As our procedure to determine the intersection time $t = t^*$ in Section 3.3 is algebraic, using a Newton iterative solver to find the root of the nonlinear equation (24), we would like to prove that this nonlinear equation has at most one root before the natural break time of the element \mathbf{e} , in order to facilitate the convergence of the Newton iteration procedure. The uniqueness of the root of (24) is equivalent to the uniqueness of the intersecting point $t = t^*$ of $S_1(t)$ and $S_2(t)$.

We prove this uniqueness by showing the monotonicity of the density values $\rho_1(t)$ (the right value of the left shock $S_1(t)$) and $\rho_2(t)$ (the left value of the right shock $S_2(t)$), see again Figure 19. By continuity of the density between the two adjacent shocks, we clearly have $\rho_1(t^*) = \rho_2(t^*)$. Furthermore, as the density profile within the element \mathbf{e} is linear, and the characteristic lines between the two adjacent shocks do not intersect, it is easy to see geometrically that $\rho_1(t)$ and $\rho_2(t)$ must be monotone with opposite trends (that is, either $\rho_1(t)$ is monotonically increasing and $\rho_2(t)$ is monotonically decreasing, or vice versa). We

will also prove this fact algebraically below. With this fact, we have clearly established the uniqueness of the intersecting point $t = t^*$ of the two shock curves $S_1(t)$ and $S_2(t)$.

Assume that the governing flux of the element \mathbf{e} is

$$q(\rho) = e_2\rho^2 + e_1\rho + e_0$$

we have, by (6)-(7), the formulas for $\rho_1(t)$ and $\rho_2(t)$:

$$\begin{aligned}\rho_1(t) &= \frac{\bar{\rho}_l\bar{x}_r - \bar{\rho}_r\bar{x}_l + e_1(\bar{\rho}_l - \bar{\rho}_r)t - (\bar{\rho}_l - \bar{\rho}_r)(S_1(t) + \bar{x}_l)}{\bar{x}_r - \bar{x}_l - 2e_2(\bar{\rho}_l - \bar{\rho}_r)t} \\ \rho_2(t) &= \frac{\bar{\rho}_l\bar{x}_r - \bar{\rho}_r\bar{x}_l + e_1(\bar{\rho}_l - \bar{\rho}_r)t - (\bar{\rho}_l - \bar{\rho}_r)(S_2(t) + \bar{x}_r)}{\bar{x}_r - \bar{x}_l - 2e_2(\bar{\rho}_l - \bar{\rho}_r)t}\end{aligned}$$

Therefore we have

$$\begin{aligned}\rho_1'(t) &= -\frac{(\bar{\rho}_l - \bar{\rho}_r)\{(e_1 + 2e_2\bar{\rho}_l)(\bar{x}_l - \bar{x}_r) + 2e_2(\bar{\rho}_l - \bar{\rho}_r)S_1(t) + [2e_2(\bar{\rho}_r - \bar{\rho}_l)t + \bar{x}_r - \bar{x}_l]S_1'(t)\}}{[2e_2(\bar{\rho}_l - \bar{\rho}_r)t + \bar{x}_l - \bar{x}_r]^2} \\ \rho_2'(t) &= -\frac{(\bar{\rho}_l - \bar{\rho}_r)\{(e_1 + 2e_2\bar{\rho}_r)(\bar{x}_l - \bar{x}_r) + 2e_2(\bar{\rho}_l - \bar{\rho}_r)S_2(t) + [2e_2(\bar{\rho}_r - \bar{\rho}_l)t + \bar{x}_r - \bar{x}_l]S_2'(t)\}}{[2e_2(\bar{\rho}_l - \bar{\rho}_r)t + \bar{x}_l - \bar{x}_r]^2}\end{aligned}$$

On the one hand $S_1'(t) > q'(\rho_1(t))$ and $S_2'(t) < q'(\rho_2(t))$, by the entropy condition. That is to say, $S_1'(t) > 2e_2\rho_1(t) + e_1$ and $S_2'(t) < 2e_2\rho_2(t) + e_1$.

On the other hand $[2e_2(\bar{\rho}_r - \bar{\rho}_l)t + \bar{x}_r - \bar{x}_l] > 0$ since we assume that time t is less than the natural break time of the element given by (21).

We now have

$$\begin{aligned}& (e_1 + 2e_2\bar{\rho}_l)(\bar{x}_l - \bar{x}_r) + 2e_2(\bar{\rho}_l - \bar{\rho}_r)S_1(t) + [2e_2(\bar{\rho}_r - \bar{\rho}_l)t + \bar{x}_r - \bar{x}_l]S_1'(t) \\ > & (e_1 + 2e_2\bar{\rho}_l)(\bar{x}_l - \bar{x}_r) + 2e_2(\bar{\rho}_l - \bar{\rho}_r)S_1(t) + [2e_2(\bar{\rho}_r - \bar{\rho}_l)t + \bar{x}_r - \bar{x}_l](2e_2\rho_1(t) + e_1) \\ = & (e_1 + 2e_2\bar{\rho}_l)(\bar{x}_l - \bar{x}_r) + 2e_2(\bar{\rho}_l - \bar{\rho}_r)S_1(t) \\ & + [2e_2(\bar{\rho}_r - \bar{\rho}_l)t + \bar{x}_r - \bar{x}_l] \left(2e_2 \frac{\bar{\rho}_l\bar{x}_r - \bar{\rho}_r\bar{x}_l + e_1(\bar{\rho}_l - \bar{\rho}_r)t - (\bar{\rho}_l - \bar{\rho}_r)(S_1(t) + \bar{x}_l)}{\bar{x}_r - \bar{x}_l - 2e_2(\bar{\rho}_l - \bar{\rho}_r)t} + e_1 \right) \\ = & (e_1 + 2e_2\bar{\rho}_l)(\bar{x}_l - \bar{x}_r) + 2e_2(\bar{\rho}_l - \bar{\rho}_r)S_1(t) \\ & + 2e_2[\bar{\rho}_l\bar{x}_r - \bar{\rho}_r\bar{x}_l + e_1(\bar{\rho}_l - \bar{\rho}_r)t - (\bar{\rho}_l - \bar{\rho}_r)(S_1(t) + \bar{x}_l)] + [2e_2(\bar{\rho}_r - \bar{\rho}_l)t + \bar{x}_r - \bar{x}_l]e_1 \\ = & 0\end{aligned}$$

and

$$\begin{aligned}
& (e_1 + 2e_2\bar{\rho}_r)(\bar{x}_l - \bar{x}_r) + 2e_2(\bar{\rho}_l - \bar{\rho}_r)S_2(t) + [2e_2(\bar{\rho}_r - \bar{\rho}_l)t + \bar{x}_r - \bar{x}_l]S_2'(t) \\
< & (e_1 + 2e_2\bar{\rho}_r)(\bar{x}_l - \bar{x}_r) + 2e_2(\bar{\rho}_l - \bar{\rho}_r)S_2(t) + [2e_2(\bar{\rho}_r - \bar{\rho}_l)t + \bar{x}_r - \bar{x}_l](2e_2\rho_2(t) + e_1) \\
= & (e_1 + 2e_2\bar{\rho}_r)(\bar{x}_l - \bar{x}_r) + 2e_2(\bar{\rho}_l - \bar{\rho}_r)S_2(t) \\
& + [2e_2(\bar{\rho}_r - \bar{\rho}_l)t + \bar{x}_r - \bar{x}_l] \left(2e_2 \frac{\bar{\rho}_l\bar{x}_r - \bar{\rho}_r\bar{x}_l + e_1(\bar{\rho}_l - \bar{\rho}_r)t - (\bar{\rho}_l - \bar{\rho}_r)(S_2(t) + \bar{x}_r)}{\bar{x}_r - \bar{x}_l - 2e_2(\bar{\rho}_l - \bar{\rho}_r)t} + e_1 \right) \\
= & (e_1 + 2e_2\bar{\rho}_r)(\bar{x}_l - \bar{x}_r) + 2e_2(\bar{\rho}_l - \bar{\rho}_r)S_2(t) \\
& + [2e_2(\bar{\rho}_r - \bar{\rho}_l)t + \bar{x}_r - \bar{x}_l]e_1 + 2e_2[\bar{\rho}_l\bar{x}_r - \bar{\rho}_r\bar{x}_l + e_1(\bar{\rho}_l - \bar{\rho}_r)t - (\bar{\rho}_l - \bar{\rho}_r)(S_2(t) + \bar{x}_r)] \\
= & 0
\end{aligned}$$

Therefore $\rho_1'(t) < 0$, $\rho_2'(t) > 0$ if $\bar{\rho}_l > \bar{\rho}_r$; and $\rho_1'(t) > 0$, $\rho_2'(t) < 0$ if $\bar{\rho}_l < \bar{\rho}_r$. The desired monotonicity is proven.

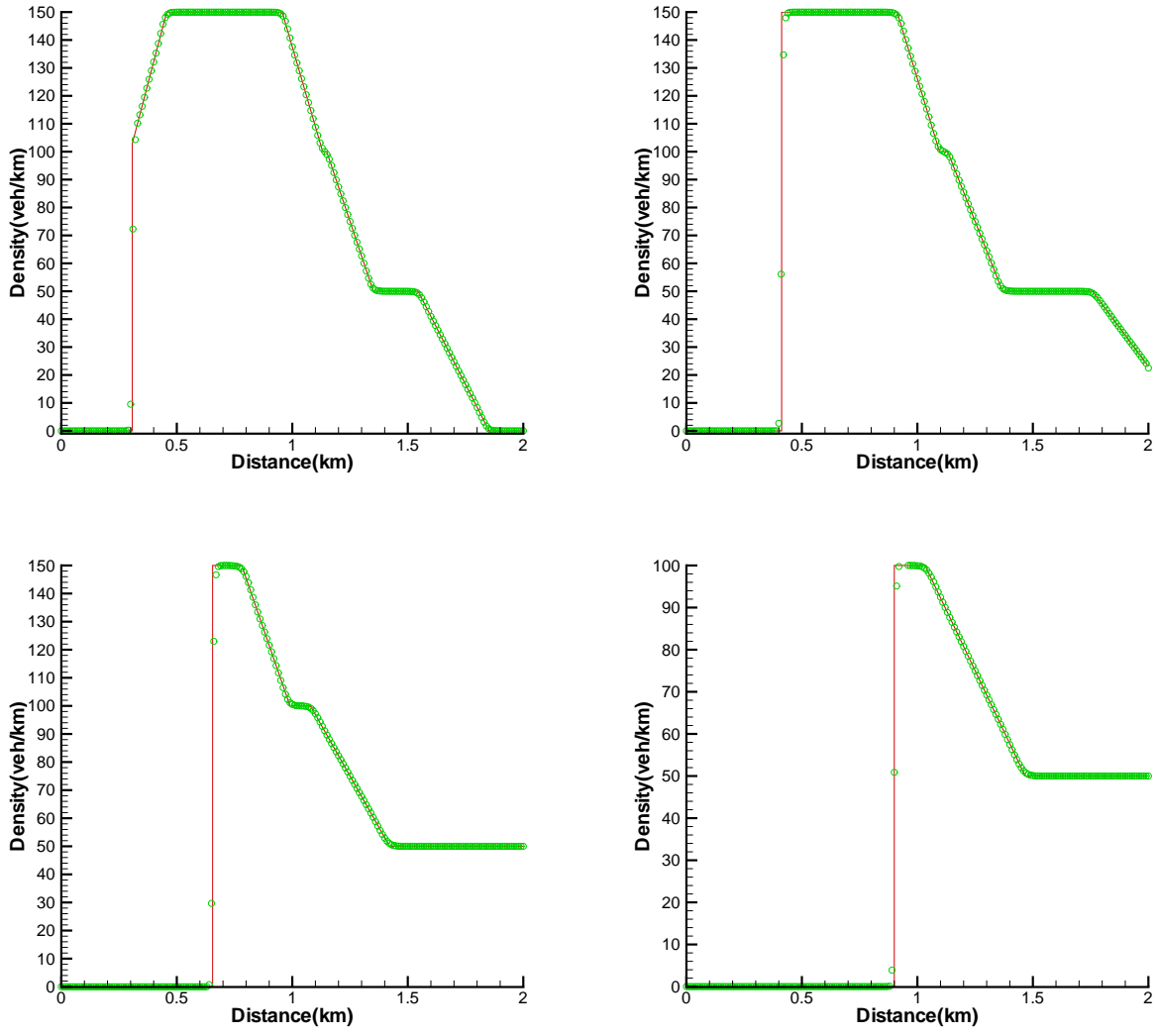


Figure 12: The exact entropy solution obtained by the procedure in this paper (solid line) and the numerical solution obtained by using a fifth order WENO finite difference scheme with $N = 200$ uniform grid points (circles). Example 1. Top left: $t = 0.2112$ min; top right: $t = 0.4245$ min; bottom left: $t = 1.060$ min; bottom right: $t = 1.600$ min.

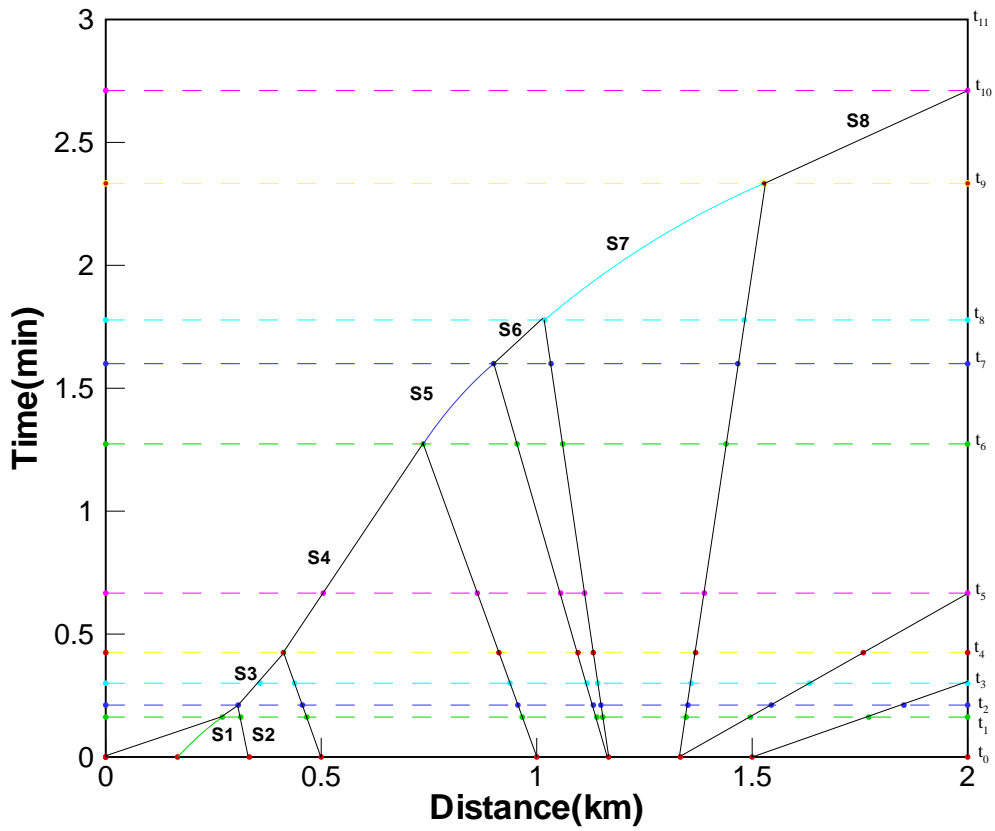


Figure 13: The time-space diagram for all waves (shocks and rarefaction waves) involved in the evolution process for Example 1 until $t = 3.0$ min.

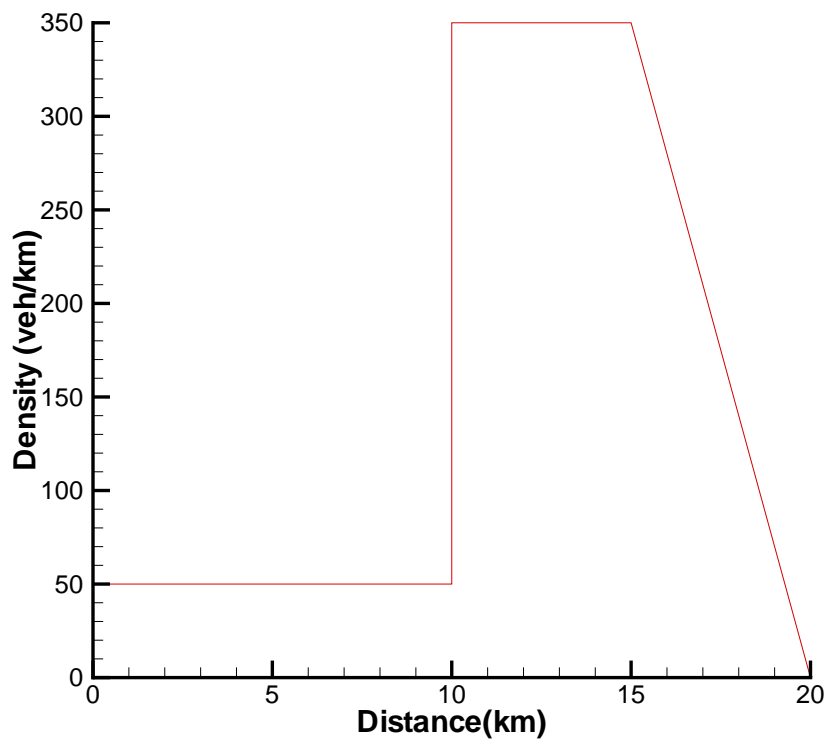


Figure 14: The initial density profile for Example 2.

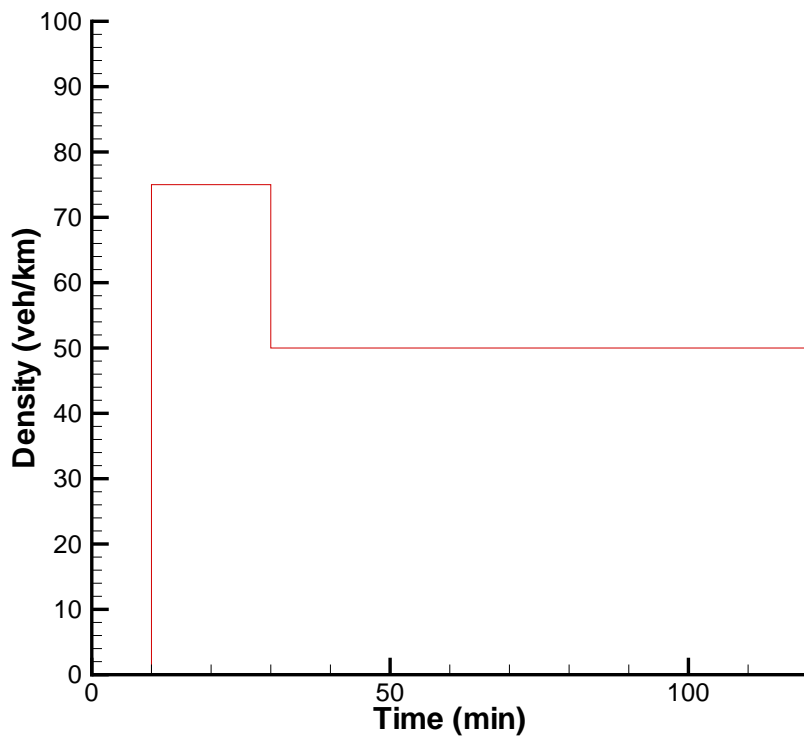


Figure 15: The density variation at the entrance in time for Example 2.

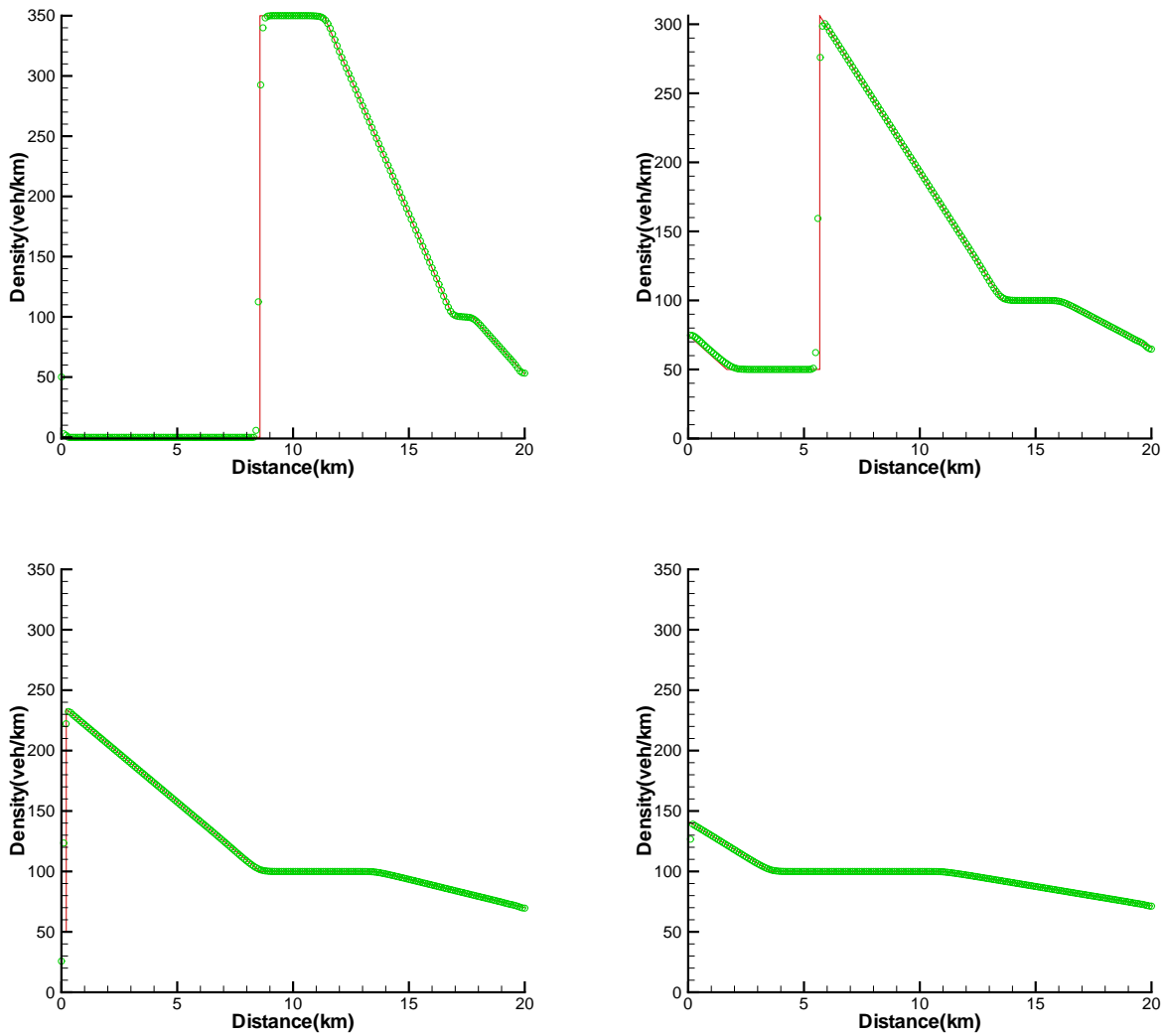


Figure 16: The exact entropy solution obtained by the procedure in this paper (solid line) and the numerical solution obtained by using a fifth order WENO finite difference scheme with $N = 200$ uniform grid points (circles). Example 2. Top left: $t = 10$ min; top right: $t = 30$ min; bottom left: $t = 60$ min; bottom right: $t = 90$ min.

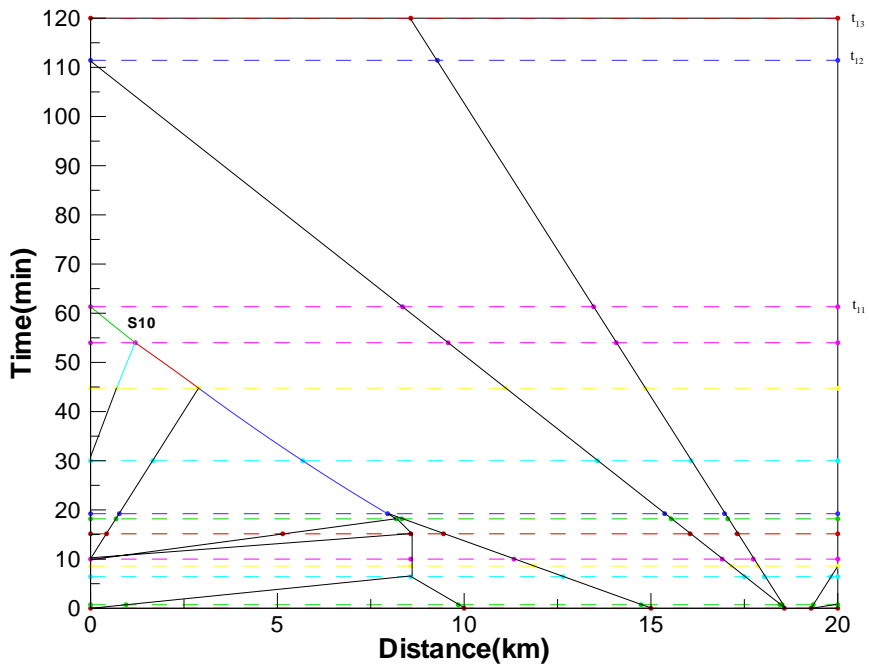
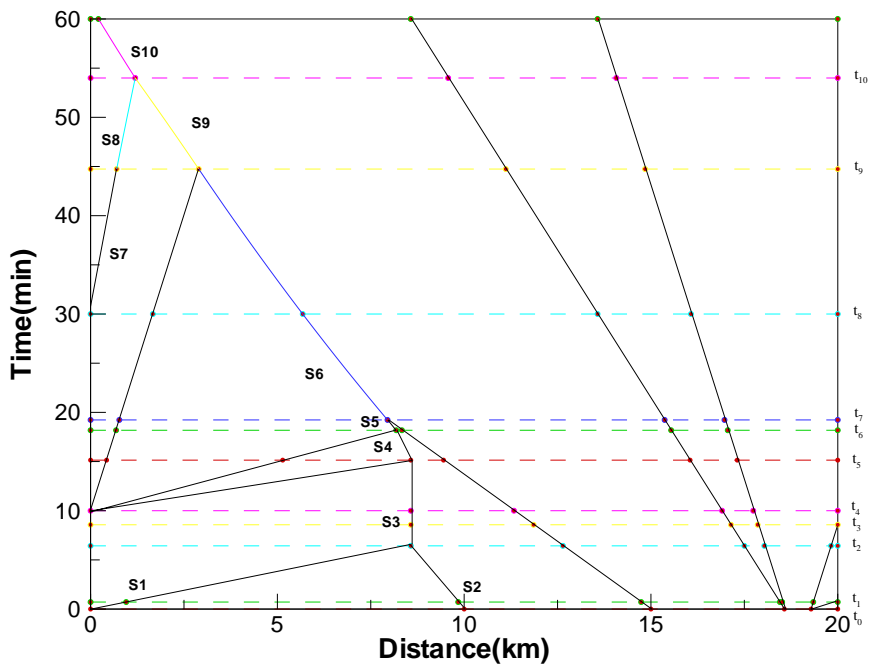


Figure 17: The time-space diagram for all waves (shocks and rarefaction waves) involved in the evolution process for Example 2 until $t = 60$ min (top) and until $t = 120$ min (bottom).

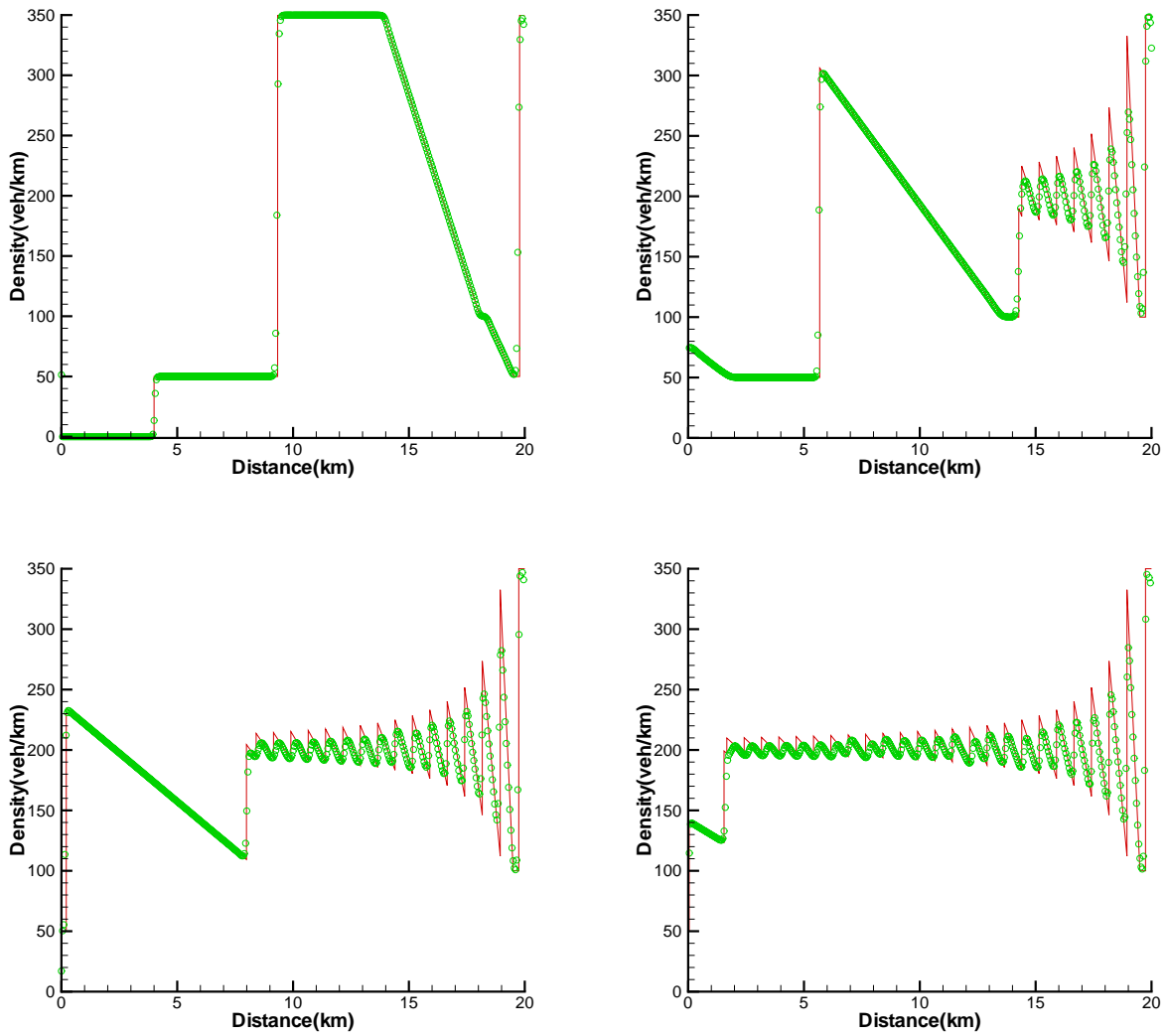


Figure 18: The exact entropy solution obtained by the procedure in this paper (solid line) and the numerical solution obtained by using a fifth order WENO finite difference scheme with $N = 400$ uniform grid points (circles). Example 3. Top left: $t = 3$ min; top right: $t = 30$ min; bottom left: $t = 60$ min; bottom right: $t = 90$ min.

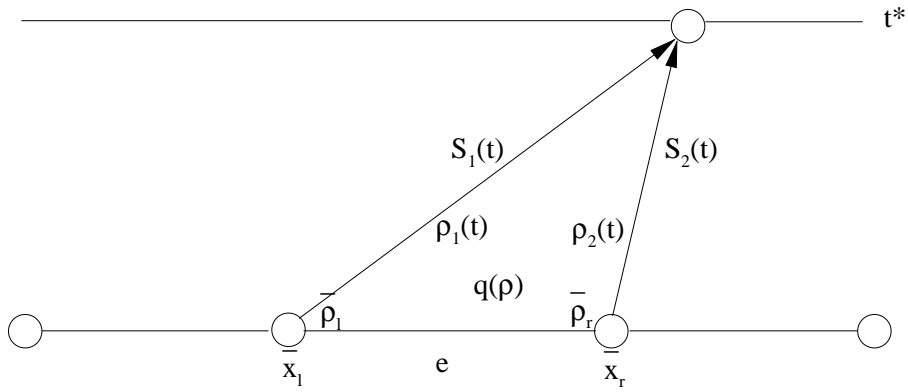


Figure 19: Two adjacent shocks intersect at time $t = t^*$.